JASN

Morphological Processes of Foot Process Effacement in Puromycin Aminonucleoside Nephrosis Revealed by FIB/SEM Tomography

Journal:	*Journal of the American Society of Nephrology*
Manuscript ID	JASN-2018-02-0139.R3
Manuscript Type:	Original Article - Basic Research
Date Submitted by the Author:	n/a
Complete List of Authors:	Ichimura, Koichiro; Juntendo University School of Medicine, Department of Anatomy and Life Structure Miyaki, Takayuki; Juntendo University School of Medicine, Department of Anatomy and Life Structure Kawasaki, Yuto; Juntendo University School of Medicine, Department of Anatomy and Life Structure Kinoshita, Mui; Juntendo University School of Medicine, Department of Anatomy and Life Structure Kakuta, Soichiro; Juntendo University School of Medicine, Laboratory of Morphology and Image Analysis Sakai, Tatsuo; Juntendo University School of Medicine, Department of Anatomy and Life Structure
Keywords:	podocyte, ultrastructure, foot process effacement, 3D electron microscopy

Oct 23, 2018

Prof. Josephine P. Briggs
Editor-in-Chief
Journal of the American Society of Nephrology

Dear Prof. Briggs:

I would like to re-submit our revised manuscript for publication in the *Journal of the American Society of Nephrology*, titled "**Morphological Processes of Foot Process Effacement in Puromycin Aminonucleoside Nephrosis Revealed by FIB/SEM Tomography**". We are grateful to you and the reviewer for the helpful comments on our original manuscript. We have responded to all the comments and edited our revised manuscript. We believe that the changes have greatly improved the manuscript and hope that this revised version of our paper is now suitable for publication in the *Journal of the American Society of Nephrology*.

Looking forward to hearing from you.

Sincerely,

Koichiro Ichimura, M.D., Ph.D.
Department of Anatomy and Life Structure,
Juntendo University Graduate School of Medicine
2-1-1 Hongo, Bunkyo-ku, Tokyo 113-8421, Japan
E-mail: ichimura@juntendo.ac.jp

Response to Reviewer

We would like to thank the reviewer #2 for their critical comments and useful suggestions, which helped us to greatly improve our manuscript. We have taken all these comments into account in the revised manuscript. We highlighted the changes in the revised manuscript in red.

REVIEWER 2

Comment

The authors have added a series of pictures that show a transcellular route as a possible leakage way for proteins. Actually, this pathway has previously been described in PAN-nephrosis by Venkatachalam and colleagues (Venkatachalam MA, Karnovsky MJ, Cotran RS. Glomerular permeability–ultrastructural studies in experimental nephrosis using horseradish peroxidase as a tracer. J Exp Med (1969) 130:381–399). This paper should be cited. The term “transpseudocystic pathway” should be deleted. The text in Results, Discussion and the legend should be accordingly changed. The uptake of horseradish peroxidase by endocytosis, its transport in vesicles and the excretion by exocytosis shown by the previous authors clearly define this kind of transport as transcellular.

Response

Following the reviewer’s comment, we have cited the paper (Venkatachalam et al., 1969) in the Result and Discussion sections (Page 12, Line XX; Page 17, Line 6). We have changed the term “transpseudocystic pathway” into “transcellular pathway” throughout the manuscript.

Original Article: JASN-2018-02-0139. R3.

Morphological Processes of Foot Process Effacement in Puromycin Aminonucleoside Nephrosis Revealed by FIB/SEM Tomography

Koichiro Ichimura[1,2*], Takayuki Miyaki[1], Yuto Kawasaki[1], Mui Kinoshita[1], Soichiro Kakuta[2], and Tatsuo Sakai[1]

[1]Department of Anatomy and Life Structure, Juntendo University Graduate School of Medicine, Tokyo, Japan; [2]Laboratory of Morphology and Image Analysis, Research Support Center, Juntendo University Graduate School of Medicine, Tokyo, Japan

Running Title: 3D ultrastructure of podocytes

Word Count (Abstract): 203 words

Word Count (Abstract, Significance Statement, and Main Text): 3340 words

***Address Correspondence to**: Dr. Koichiro Ichimura, Department of Anatomy and Life Structure, Juntendo University Graduate School of Medicine, 2-1-1 Hongo, Bunkyo-ku, Tokyo 113-8421, Japan. Email: ichimura@juntendo.ac.jp

Keywords:

FIB/SEM tomography, podocyte, foot process effacement, autocellular junction.

Author Contributions:

KI designed the experiments. KI and SK obtained the serial FIB/SEM images. KI, TM, YK,

and MK performed 3D reconstruction. KI and TS analyzed the experimental data. KI prepared the figures and wrote the manuscript text.

SIGNIFICANCE STATEMENT

Although foot process effacement is a known pathological marker of podocyte injury, its morphological development has not been elucidated. To clarify the 3D morphology during foot process effacement, we analyzed reconstructed puromycin nephrotic podocytes made from serial, sectional focused-ion beam/scanning electron microscopy (FIB/SEM) images. The high-quality 3D reconstructed images enabled the successful description of the 3D morphological changes during foot process effacement and its associated alterations such as fragmentation, autocellular tight junctions, and ridge-like prominence retraction, in greater detail than has been described based on conventional electron microscopy.

ABSTRACT

Background: Foot process effacement is one of the pathological indicators of podocyte injury. However, the morphological changes associated with it remain unclear.

Methods: To clarify the developmental process, we analyzed puromycin nephrotic podocytes reconstructed from serial focused-ion beam/scanning electron microscopy (FIB/SEM) images.

Results: Intact podocytes consisted of four subcellular compartments: cell body, primary process, ridge-like prominence (RLP), and foot process. The RLP, a longitudinal protrusion from the basal surface of the cell body and primary process, served as an adhesive apparatus for the cell body and primary process to attach to the glomerular basement membrane. Foot processes protruded from both sides of the RLP. In puromycin nephrotic podocytes, foot process effacement occurred in two ways; by type-1 retraction, where the foot processes retracted while maintaining their rounded tips or type-2 retraction, where they narrowed across their entire lengths, tapering toward the tips. Puromycin nephrotic podocytes also exhibited several alterations associated with foot process effacement, such as deformation of the cell body, retraction of RLPs, and cytoplasmic fragmentation. Finally, podocytes were reorganized into a broad, flattened shape.

Conclusion: The 3D reconstruction of podocytes based on serial FIB/SEM images

revealed the morphological changes involved in foot process effacement in greater detail than previously described.

INTRODUCTION

Podocytes, which are complicated epithelial cells specialized for glomerular ultrafiltration, contain at least three different subcellular compartments: the cell body, primary process, and foot process.[1] The foot processes are the adhesive apparatus of podocytes that allow attachment to the glomerular basement membrane (GBM). Foot processes interdigitate with those of the neighboring podocytes. The primary processes are the connecting structure between the cell body and the foot processes. Conventional scanning electron microscopy (SEM) is a useful method for exploring the compartmental structures of podocytes.[2-4] However, conventional SEM does not sufficiently reveal the complete architecture of individual podocytes, because it does not allow observation of the basal surface of the cells.

To reveal the precise architecture of podocytes, we previously examined intact podocytes reconstructed from serial sectional images of the glomerulus acquired using focused-ion-beam (FIB)/SEM tomography (See the details of this technique in **Supplementary Fig. 1**).[5-7] The reconstructed podocytes revealed that a more accurate structural hierarchy of subcellular compartments includes the “ridge-like prominence” (RLP), which protrudes directly from the basal surface of the cell body and primary process (**Supplementary Fig. 2**). This subcellular compartment has been already recognized using conventional SEM and transmission electron microscopy (TEM) and is

referred to as the “central foot process” or “anchoring (foot) process”. [8-10] Our 3D structural analysis using FIB/SEM tomography further cleared that the RLPs serve as an adhesive apparatus for the cell body and primary process to attach to the GBM and as a connecting structure for attaching the foot processes to the cell body or primary processes.[6, 11] Furthermore, reconstructed podocytes also clearly showed cytoplasmic arcades—the anastomosis between two primary processes from the same podocyte.[5, 12] Similar to primary processes, the cytoplasmic arcades also contained RLPs and foot processes (**Supplementary Figs. 3** and **4**).

In glomerular diseases, podocytes lose the usual interdigitating pattern of foot processes between neighboring podocytes, and this alteration, known as “foot process effacement,” is regarded as a pathological indicator of podocyte injury.[12-14] The morphological processes of foot process effacement have been elucidated to a limited extent using conventional SEM;[12, 13, 15] some morphological aspects remain unclear owing to the technical limitations of conventional SEM.

In the present study, to clarify the morphological processes of foot process effacement, we used FIB/SEM tomography to examine diseased podocytes in puromycin aminonucleoside (PAN) nephrosis rats, an animal model of minimal change nephrotic syndrome in humans. We successfully described the morphological processes involved in foot process effacement in greater detail than has been previously described using

conventional SEM.

METHODS

PAN Nephrosis

To induce PAN nephrosis, we intraperitoneally administered PAN (15 mg/100 g body weight; Sigma-Aldrich, St. Louis, MO, USA) to 6-week-old male Wistar rats (Charles River Japan, Yokohama, Japan). Animals were perfused with 2.5% glutaraldehyde/0.1 M phosphate buffer under anesthesia with pentobarbital on day 1, 2, 4, and 8. As a control, we used 6-week-old male Wistar rats that were not administered PAN. All procedures performed on the laboratory animals were approved by the Institutional Animal Care and Use Committee of Juntendo University School of Medicine (Approval No. 290213).

Conventional SEM

Conventional SEM was performed as described previously.[16]

FIB/SEM Tomography and 3D Reconstruction

Fixed kidney tissues were stained and embedded in Epoxy resin as described previously.[6] From three glomeruli in each experimental group, serial FIB/SEM images were obtained at 50-nm increments using a backscattered electron detector at a 2.0-kV acceleration

voltage using a Helios Nanolab 660 FIB/SEM (Thermo Fisher Scientific, Waltham, MA, USA). The pixel size of each FIB/SEM image was 13.5 × 17.1 × 50 nm/pixel (width × height × depth). The pixel dimensions for a recorded image were 3072 × 2048 pixels. Thus, the dimension of the serial image acquired using FIB/SEM was 41.5 × 35.0 × 20–35 μm (width × height × depth). The new surface for serial FIB/SEM imaging was generated using FIB-milling with a 0.77-nA beam current, where gallium ions were accelerated at a voltage of 30 kV. The 3D reconstruction of podocytes was performed using an AMIRA 6.1 software (Thermo Fisher Scientific).

Statistical Analysis

All measurements are shown as means ± standard error of the mean (SE). Differences were tested using ANOVA followed by the Bonferroni test as post hoc test; $P < 0.05$ was considered statistically significant.

RESULTS

Structural Alterations in PAN Nephrotic Podocytes Observed by Conventional SEM

To observe the outline of the structural alterations in PAN nephrotic podocytes, we first observed them using conventional SEM (**Fig. 1**). In control (normal) podocytes, the cell body projected primary processes, which protruded numerous fine foot processes that

interdigitated with those of the neighboring podocytes (**Fig. 1A1** and **A2**). Some primary processes bifurcated two or three times—we referred to the portions distal to the first bifurcation as primary processes, and not as secondary and tertiary processes in this study.

In the pre-proteinuria phase (day 2), numerous fine foot processes were still found between the primary processes (**Fig. 1B1**). Numerous microvilli and bleb-like protrusions appeared on the cell body and primary processes (**Fig. 1B1** and **B2**). In the overt proteinuria phase (day 4), the primary processes became irregular in shape and were significantly broadened compared with those of the control rats (**Fig. 1C1** and **C2**; **Supplementary Fig. 5**); thus, the space between the primary processes narrowed considerably.

Moreover, the periphery of the cell body extended between the primary processes to form what appeared to be webbing, creating broad and flattened podocytes (arrows in **Fig. 1C1** and **C2**). The foot processes were almost hidden under the deformed cell bodies and primary processes; thus, it was difficult to clarify the morphological processes of the foot process effacement only using conventional SEM, although this method was useful for observing the alterations in the luminal surface structure of cell bodies and primary processes. To overcome this problem, we next analyzed the podocytes reconstructed from the serial FIB/SEM images.

Foot Process Effacement in PAN Nephrotic Podocytes Revealed by FIB/SEM Tomography

Reconstructed podocytes could be observed from any perspective, and the basal view was particularly useful in understanding the alterations in the foot processes (**Fig. 2**). From the reconstructed podocytes, we found two forms of foot process effacement, type-1 and type-2 retractions, during the progression of PAN nephrosis (**Fig. 3**). In normal podocytes, the foot processes exhibited a relatively uniform width at the base, except at the enlarged terminal portions (**Fig. 2A**). In type-1 retraction, the foot processes were shortened while losing their width uniformity but maintaining their rounded tips (**Fig. 3A1**–**3** and **C**). The loss of width uniformity and shortening were found in most of the foot processes on day 1 (**Figs. 2B1**, **2B2**, and **3E**), indicating that type-1 retraction had already initiated from as early as day 1.

In type-2 retraction, the foot processes were shortened, extremely narrowed across their entire lengths, and tapered toward the tips (**Fig. 3B1**–**3**, **C**, and **F**). Type-2 retraction was also observed on day 1 (**Fig. 2B2**); however, unlike type-1 retraction, it was found only in some foot processes. At this point, it was not clear whether the two types of foot process retraction progressed independently or they represented two different phases of the same phenomenon of foot process effacement.

According to the foot process effacement in each podocyte, the neighboring podocytes altered their structure to maintain their intercellular junctions, including the slit diaphragm (SD) and tight junction (TJ). In both type-1 and type-2 retractions, the neighboring podocytes exhibited widened RLPs (arrowheads in **Fig. 3D1, and D2**). In type-2 retraction, the neighboring podocytes further extended their primary processes over the retracting foot processes as a roof (arrowheads in **Fig. 3B3**; arrows in **Fig. 3D2**).

Structural Alterations Associated with Foot Process Effacement Revealed by FIB/SEM Tomography

Serial FIB/SEM and 3D reconstructed images further revealed the structural alterations associated with foot process effacement, in addition to the deformation of the cell body and primary processes shown by conventional SEM.

RLP retraction

The RLPs were widened because of the foot process retraction as described above. However, some of the RLPs lost most of their foot processes and narrowed to retract (arrows in **Fig. 4A1**, **A2**, and **C**). Consequently, the two neighboring primary processes on both sides of the retracting RLP expanded, and thus the denuded GBM did not appear by the RLP retraction (arrowheads in **Fig. 4A1** and **D**). These expanded primary

processes were connected by a newly formed TJ (arrowhead in **Fig. 4E1–4**). If the expanded primary processes were derived from the same podocyte cell body, they formed an autocellular TJ (aTJ) to connect to each other (arrowheads in **Fig. 5**), which has never been observed in normal podocytes. RLP retraction was observed below the cell body (**Fig. 4**), the proximal part of the primary processes (**Fig. 5**), and the cytoplasmic arcades (**Supplementary Fig. 6**).

Cytoplasmic fragment (CF) formation

The CFs were identified as a podocyte fragment without connection to neighboring podocytes. Unlike previously discovered podocyte fragments, the CF was in contact with the GBM along with the neighboring podocyte (yellow masses in **Fig. 6**). The CFs, which were of variable size and shape, frequently appeared both in the pro-proteinuria and overt proteinuria phases, although the dropout of an entire podocyte was not observed in this study.

The CFs were classified into three types based on their positional relationship to the neighboring podocyte: type-1 CFs were covered by the deformed cell body or primary process (**Fig. 6A1–4**), type-2 CFs penetrated the deformed primary process (**Fig. 6B1–4**), and type-3 CFs were surrounded by two deformed primary processes (**Fig. 6C1–4**), and their distal ends were connected by the aTJ (arrows in **Fig. 6C1–3** and **C5**).

We found several CFs that were shedding into the urinary space (**Supplementary Fig. 7**). The adhesive area of such CF to the GBM became very small. However, there was no gap between the shedding CF and the neighboring podocytes. This finding indicated that the neighboring podocyte extended and covered the GBM in response to the shedding of CF.

Alterations of podocyte intercellular junctions

As an initial alteration, the SD moved towards the luminal side, and the TJ appeared and coexisted beneath the SD (arrowheads in **Fig. 7E**, **F**), as reported previously.[17] This phenomenon occurred on day 1 to 4. Part of the SD moved further toward the luminal side without any association with the TJ and held its position as an ectopic SD (eSD) between the deformed primary processes. Some eSD were located between a pair of cup-shaped protrusions derived from two neighboring primary processes (**Fig. 7A**–**E**), whereas others were between the smooth surfaces of the deformed primary processes.

On day 8, the podocytes were predominantly connected to each other by the TJs, except for the eSD (**Fig. 7G1** and **G2**). Moreover, we found some intercellular gaps without any junctional apparatuses in this stage (arrows in **Fig. 8A1** and **A2**; **Supplementary Fig. 8**). These intercellular gaps and micro-denudation of the GBM associated with them presumably functioned as a protein-leakage pathway, which should be called “intercellular

pathway"

Pseudocyst formation

The PAN nephrotic podocytes exhibited numerous pseudocysts within their deformed cell bodies and primary processes on day 4 and 8, when severe proteinuria was recognized (**Fig. 8C1**, **D**, **E1**; **Supplementary Figs. 9** and **10**), as described in previous electron microscopic studies.[18-21]

Serial FIB/SEM images revealed that the pseudocysts were topologically divided into following three types: type-1 pseudocysts were dome-shaped and outpocketing, developing in conjunction with focal micro-denudation of the GBM (**Fig. 8C1** and **C2**; **Supplementary Fig. 9**); type-2 pseudocysts were completely closed (**Fig. 8D**; **Supplementary Fig. 9**); and type-3 pseudocysts were opened to the urinary space through small channels (**Fig. 8E1** and **E2**; **Supplementary Fig. 10**). The types-1 and -2 pseudocysts frequently contained amorphous materials, which is reminiscent of the plasma protein aggregation due to chemical fixation; whereas type-3 pseudocysts did not contain any such amorphous materials. These pseudocysts presumably contributed to another protein-leakage pathway, which should be called "transcellular pathway" (see Discussion).

DISCUSSION

Advantages of FIB/SEM Tomography in Structural Analysis of Podocytes

FIB/SEM tomography, including reconstruction technique, enabled a more precise analysis of the 3D ultrastructure of healthy, developing, and diseased podocytes, as shown in our present and previous studies.[5-7, 22]

The high level of visibility of the 3D ultrastructure is the most important advantage of this method. Conventional SEM is useful for revealing the luminal surface structure of podocytes; however, it is too weak to directly observe several portions of the podocytes, such as the basal surface structures. The 3D reconstruction images of single podocytes based on FIB/SEM tomography completely overcame this problem by enabling the observation of surface structures from any direction and without interpretation by neighboring podocytes or GBM. Furthermore, the color-coded reconstruction images of multi-podocytes are also valuable for analyzing the 3D mutual relationship of podocytes.

In FIB/SEM tomography, numerous serial FIB/SEM images of podocytes, which achieve quality comparable to that of conventional TEM images, can be easily observed. This feature is another advantage of FIB/SEM tomography in the 3D ultrastructural analysis of podocytes. By observing the serial FIB/SEM images, we could analyze two potential leakage pathways for plasma proteins in the PAN nephrotic podocytes.

Pathological Significance of aTJ and eSD in Podocytes

The aTJ, a connection between two adjacent parts of the same cell mediated by the same adhesion complex,[16] has not been reported in vertebrate podocytes. However, the PAN nephrotic podocytes formed aTJs, especially in the overt proteinuria phase. This formation of the aTJ contributes to preventing the exposure of the GBM caused by the retraction of podocyte protrusions.

In PAN nephrosis, proteinuria gradually becomes less severe over a period of several months, but glomeruli are not completely restored to normal morphology.[23, 24] Several possibilities have been considered regarding the fate of the podocyte aTJ after restoration. For instance, if a long aTJ persists in the recovery phase, it is highly likely to interfere with the restoration of the normal architecture of podocytes. In this study, we did not analyze the recovery phase of PAN nephrosis. In a future study, to determine the effect of aTJs on podocyte restoration, we will examine whether aTJs are retained in the recovery phase and the extent to which deformed podocytes can be restored to the normal architecture.

The eSD between the primary processes clearly do not contribute to the filtration barrier function. However, they may play a role in the pool of SD proteins used to restore normal SDs at the base of foot processes.

Formation and Fate of CFs in PAN Nephrotic Podocytes

It is reasonable to think that the CFs were derived from the distal parts of foot processes or primary processes with their foot processes. Type-1 CFs were formed by the separation of the distal parts under the deformed cell body and primary processes of neighboring podocyte. Type-1 CFs were highly likely to necrotize under the neighboring podocyte; however, it was difficult to clarify the fate of type-1 CFs from the data obtained in this study.

Type-2 CFs were presumably derived from the distal parts of the podocytes in the fenestration surrounded by the cytoplasmic arcade and its parental primary processes. The cytoplasmic arcade possessed RLPs that continued and joined those of the parental primary processes; thus, the fenestration was also surrounded by a continuous RLP. The continuous RLP possessed one narrow channel to allow the neighboring podocyte to enter the fenestration (yellow lines in **Supplementary Fig. 3**). The neighboring podocyte broke off at the narrow channel, converting the part in the fenestration to a type-2 CF. Thus, the distal regions of podocytes that entered into the fenestration can be regarded as a “fragile region” in podocytes.

Type-3 CFs were presumably formed by the separation of the distal parts of podocytes that were located between two primary processes from the same neighboring podocyte. After the separation, the primary processes next to the CF expanded and connected with the aTJ.

Most of the Type-2 and -3 CFs were highly likely to shed into the urinary space. In this study, we found three shedding type-2 CFs, which were shed into the urinary space without forming intercellular gaps. This finding indicated that the shedding CFs did not contribute to forming the bare area of the GBM as a leakage pathway for plasma proteins.

Some of the CFs appeared viable in the FIB/SEM images. The PAN nephrotic podocytes showed upregulated expression of connexin 43, a gap junction protein.[25] If gap-junction communication was established between such viable CFs and neighboring podocytes by connexin 43, this would contribute to the survival of the CFs.

Protein Leakage Pathways in PAN Nephrosis

In the present FIB/SEM analyses, at least one protein leakage pathway, “intercellular pathway”, was determined in the PAN nephrotic podocytes. The intercellular pathway consisted of the intercellular gaps without any junctional structures (SD and TJ) between deformed podocytes and the micro-denudation of GBM at the intercellular gaps.

Kriz and colleagues proposed that the pseudocysts provide a communicating system of extracellular spaces through which the filtrate pass to directly reach the urinary space.[13, 26, 27] However, we scarcely found any pseudocysts that directly communicated the micro-denudation of GBM and urinary space in the PAN nephrotic podocytes. The pseudocysts exhibited three kinds of state; if the pseudocysts shifted between the types in order of type

1, type 2, and type 3, as shown in **Fig. 8F**, they were regarded as another pathway of protein leakage, which may be called "transcellular pathway", as described by Venkatachalam *et al.* (1969). [21]

More specifically, the transcellular pathway is a consequence of the following phenomena: 1) The deformed cell body and primary processes partially detach from the GBM as the initial step of this pathway; 2) Type-1 pseudocysts are subsequently formed and developed by the filtration pressure on the detached basal surface of podocyte; 3) Developed type-1 pseudocysts lose the orifice from which the filtrate entered and become type-2 pseudocysts. Types-1 and -2 pseudocysts contained amorphous materials, which were highly likely to represent the plasma proteins leaking from the denuded area of GBM; 4) Type-2 pseudocysts coalesce with each other into large pseudocysts; 5) Enlarged type-2 pseudocysts open to the urinary space via newly-formed small channels and become type-3 pseudocysts. The leaked plasma proteins within the pseudocysts are released from the small channels into the urinary space.

Limitations of 3D Ultrastructural Analysis Using FIB/SEM Tomography

FIB/SEM tomography is a powerful tool for precisely analyzing the 3D ultrastructure of podocytes; however, there are several technical disadvantages to this method. Firstly, the imaged region is completely lost because of FIB-milling. Moreover, the non-imaged region

adjacent to the imaged region is severely damaged during scanning for the positional correction of FIB-milling. This damage makes it impossible to obtain FIB/SEM images with sufficient quality for the 3D reconstruction of foot processes. Therefore, we hesitated to adapt FIB/SEM tomography for irreplaceable specimens such as renal biopsy specimens from patients. Array tomography is a potential solution to this problem, and it was used to obtain serial images from serial ultrathin sections mounted on bases, such as silicon wafer and glass plate (**Fig. 9**).[28-31] These serial ultrathin sections are physically stable and repeatedly observable. For long-term future studies, we aim to establish a "serial ultra-thin section library" of renal biopsy specimens and to analyze them using array tomography.

CONCLUSION

FIB/SEM tomography was shown to be a powerful tool for elucidating the 3D architecture of podocytes. Using this method, we analyzed and described the morphological processes involved in foot process effacement more clearly and precisely than that reported previously. The morphological information revealed in this study will be valuable for the 3D structural analyses of podocytes in other animal and human glomerular diseases.

ACKNOWLEDGMENTS

The authors wish to thank Mr. Takanobu Ishimura (Maxnet Co., Ltd., Tokyo, Japan) for giving a technical lecture on the reconstruction software and Mr. Kota Kato (Juntendo University) for 3D printing. This study was supported, in part, by a Grant-in-Aid for Scientific Research from the Ministry of Education, Culture, Sports, Science, and Technology of Japan (MEXT, No. 15K18960, 17K08521 to KI) and Grants-in-Aid from the Foundation of Strategic Research Projects in Private Universities from the MEXT (No. S1311011, S1101009 to Juntendo University).

SUPPLEMENTARY INFORMATION (TABLE of CONTENTS)

Suppl. Fig. 10. Type-3 pseudocyst shown in PAN nephrotic podocyte.

DISCLOSURE

None.

FIGURE LEGENDS

Figure 1. Structural alterations in puromycin aminonucleoside (PAN) nephrotic podocytes observed using conventional scanning electron microscopy (SEM)

(**A1** and **A2**) Healthy (control) podocytes. The cell body projected primary processes, which protruded numerous fine foot processes that interdigitated with those of the neighboring podocytes. Some primary processes bifurcated two or three times—we referred to the portions distal to the first bifurcation as primary processes, and not as secondary and tertiary processes in this study. (**B1** and **B2**) Pre-proteinuria phase (day 2). Numerous microvilli and bleb-like protrusions appeared on the cell body and primary processes. (**C1** and **C2**) Overt proteinuria phase (day 4). The primary processes were flattened. The periphery of the cell body extended between the flattened primary processes similar to the webbing of waterfowl (green arrows). The space between the flattened primary processes narrowed considerably. The cytoplasmic arcades and their parental primary processes also became more recognizable (arrowheads in **A2**, **B2**, and **C2**). Asterisks indicate regions surrounded by the cytoplasmic arcade and its parental primary processes. CB, cell body; PP, primary process. Scale bars: 5 μm.

Figure 2. Structural alterations in basal surfaces of podocytes revealed by focused-ion-beam/scanning electron microscopic tomography

Individual podocytes are shown in different colors. The basal view of the reconstructed podocytes is useful to analyze structural alterations in the foot processes. In healthy (control) podocytes, foot processes exhibited a uniform width (**A**). Puromycin aminonucleoside (PAN) nephrotic podocytes lost this uniformity in the foot processes from day 1 (**B1** and **B2**). The uniformity in width was further lost on days 2 (**C**) and 4 (**D**). The podocytes formed a large adhesive surface on day 8, although short interdigitating processes remained (**E**). The yellow masses represent the cytoplasmic fragments of podocyte (**E**), which are frequently found in the PAN nephrotic glomeruli. Scale bar: 2 μm.

Figure 3. The two mechanisms of foot process effacement

(**A1**–**3** and **B1**–**3**) Basal view. (**A1**–**3**) Type-1 retraction. The foot processes of the neighboring green and purple podocytes retracted simultaneously but maintained their rounded tips. The ridge-like prominences of both podocytes also widened (asterisks) and prevented exposure of the glomerular basement membrane. (**B1**–**3**) Type-2 retraction. Some foot processes narrowed over their total length and tapered toward the tip (green podocyte, arrows in **B1** and **B2**). The neighboring purple podocyte displayed an overhang on the retracting foot processes of the green podocyte (arrowheads in **B3**). (**C**) Schematic drawings representing the two types of foot process effacement. Basal view. (**D1** and **D2**) Schematic drawings representing alterations in the podocyte next to the retracting

podocyte. Cross section. The purple podocyte exhibits foot process retraction. In both types-1 and -2 retraction, the neighboring (green) podocyte widened its ridge-like prominence (RLP) (arrowheads in **D1**). In type-2 retraction, the green podocyte further extended its primary process over the retracting foot process as a roof (arrows in **D2**). The slit diaphragms (SD) are replaced by the tight junctions (TJ). (**E**) Mean length of foot processes significantly decreases by type-1 retraction from day 1 with progression of PAN nephrosis: control, 1.86 ± 0.08 μm; day 1, 1.67 ± 0.06 μm; day 2, 1.57 ± 0.08 μm; day 4, 1.56 ± 0.07 μm; day 8, 1.12 ± 0.05 μm (n = 60 foot processes from three podocytes). Values are means ± standard error of the mean. Differences were tested using ANOVA followed by the Bonferroni test as post hoc test. *P < 0.05. (**F**) Focused-ion-beam/scanning electron microscopic image of type-2 retracting foot processes shown in **B1** and **B2** (arrowheads). CB, cell body; FP, foot process; PP, primary process. Scale bars: 1 μm.

Figure 4. Retraction of ridge-like prominence (RLP)

(**A1**) Basal view. The RLP of the green podocyte cell body lost their foot processes (arrows). This RLP was partially retracting and, thus, the neighboring purple and blue podocytes were directly contacted (arrowheads). (**A2**) Basal view. The blue podocyte was removed from **A1** to show the retracting RLP (arrows). (**B1** and **B2**) Schematic diagrams

showing the predicted original (**B1**) and observed (**B2**) shapes of the green podocyte shown in **A1** and **A2**. The yellow structures in B1 and B2 represent the normal or deformed RLP, respectively. The retracting RLP is shown by arrows in **A2** and **B2**. (**C**) Luminal view. The retracting RLP of the green podocyte showing **A1** and **A2** (arrows). (**D**) Luminal view. The neighboring purple and blue podocytes expanded from both sides of the retracting RLP—thus the denuded GBM do not appear by the retraction of RLP (arrowheads). (**E1**–**4**) Schematic diagrams showing RLP retraction between two different podocytes (blue and purple) and the associated intercellular tight junction (iTJ) formation by the retraction. **E3** and **E4** represent the sections at the sites indicated by the two double arrows in **A1**. CB, cell body; FP, foot process; GBM, glomerular basement membrane; SD, slit diaphragm. Scale bars: 500 nm.

Figure 5. Autocellular tight junction (aTJ) formation by retraction of ridge-like prominence (RLP)

(**A1**–**3**) Basal view. (**A1**) The aTJs existed between two deformed primary processes of the green podocyte (PP1 and PP2) (arrowheads in **A1**)—these aTJs were presumably formed by the RLP retraction in the purple podocyte. Arrows indicate remaining RLPs. (**A2**) The green podocyte was removed from **A1,** and its position is indicated by the green lines. Yellow arrows, the remaining RLP; arrowheads, the sites of aTJs between deformed

primary processes of the green podocyte. It was not determined whether the three blue regions belonged to the same podocyte or not. (**A3**) Magnification of the remaining RLP shown in **A2** (arrows). (**B1** and **B2**) Luminal view of the same green podocyte shown in **A1**. Arrowheads indicate the aTJs between PP1 and PP2 (**B1**). The cell body of the purple podocyte (CB) was positioned above the aTJ of the green podocyte (**B2**). (**C**) Focused-ion beam/scanning electron microscopy image showing an aTJ of the green podocyte (arrows). (**D**) Schematic diagrams showing aTJ formation associated with RLP retraction. FP, foot process; iTJ, intercellular tight junction; SD, slit diaphragm. Scale bars: 1 μm.

Figure 6. The three types of podocyte cytoplasmic fragments (CFs)

(**A1**, **A2**, **B1**, **B2**, **C1**, and **C2**) Basal view. The CFs are represented as yellow masses. (**A2**, **B2**, and **C2**) The CFs were removed to show their positions in relation to the neighboring purple podocyte. Asterisks indicate the space for CF. (**B3** and **C3**) Luminal view. (**A1** and **A2**) Type-1 CFs. A large CF (CF in **A1**) was completely covered by a deformed purple podocyte. Arrowheads indicate two small type-1 CFs. (**B1**–**3**) Type-2 CFs. A large CF (CF in **B1**) penetrated the deformed purple podocyte. Arrowheads indicate two small type-1 CFs. (**C1**–**3**) Type-3 CFs. CF surrounded by two deformed primary processes of purple podocyte, whose distal ends were connected by an autocellular tight junction (aTJ, arrows). (**A3**, **A4**, **B4**, **C4**) Focused-ion-beam/scanning

electron microscopy (FIB/SEM) images of CFs shown in **A1**, **B1**, and **C1**. (**C5**) FIB/SEM image of aTJ in purple podocyte (arrow). Scale bars: 1 μm.

Figure 7. Alterations of podocyte intercellular junctions

(**A**–**F**) Day 4. (**A**, **B**, **D**, and **E**) Luminal view. The slit diaphragm (SD, pink) and tight junction (TJ, yellow) were put on the reconstructed green podocytes. In some parts, the SD coexisted on the TJ (arrowheads in **E**). Part of the SD moved further toward the luminal side without associating with the TJ and held its position as an ectopic SD (eSD) between a pair of cup-shaped protrusions (asterisks in **A**, **B**, **E**) derived from two neighboring primary processes. (**C**) Focused-ion-beam/scanning electron microscopy (FIB/SEM) image of the cup-shaped protrusions (asterisk) linked by eSDs (arrows). (**D**) To clearly show the junctional apparatus, the green podocyte was removed from **A**. (**F**) FIB/SEM image of the slit diaphragm (pink arrowheads) coexisting with the tight junction (yellow arrowheads). (**G1** and **G2**) Day 8. Luminal view. The podocytes were predominantly connected to each other by the TJs (yellow). GBM, glomerular basement membrane. Scale bars: 200 nm in **C** and **F**; 500 nm in **A**, **B**, **D**, **E**, and **F2**

Figure 8. Leakage pathways for plasma proteins

(**A**, **B**) Intercellular pathway shown by focused-ion beam/scanning electron microscopy

(FIB/SEM) images. This pathway was found between purple and green podocytes as the intercellular spaces/gaps without presence of any junctional apparatus (arrows). (**C1**, **C2**, **D**, **E1**, **E2**) Three types of pseudocyst shown by FIB/SEM images. Pseudocysts were formed within the purple podocyte. Type-1 pseudocyst opened toward the glomerular basement membrane (arrow in **C1**); type-2 pseudocysts were completely closed (**D**); type-3 pseudocysts opened to the urinary space via small opening (arrow in **E1**). The types-1 and -2 pseudocysts frequently contained amorphous materials; whereas type-3 pseudocysts did not contain any amorphous materials. The openings of type-1 and type-3 pseudocysts are magnified in **C2** and **E2**, respectively. The serial FIB/SEM images containing **C1**, **D**, **E1** are shown as **Supplementary Figs. 8**, **9**, **10**, respectively. (**F**) Transcellular pathway shown by a schematic diagram. This pathway is presumably formed by the transition between pseudocystic types in the order of type 1, type 2, and type 3. CL, capillary lumen; US, urinary space. Asterisks indicate lumen of the pseudocysts; yellow lines indicate the glomerular basement membrane. Scale bars: 500 nm in **A** and **B**; 1 μm in **C1**, **D**, **E1**.

Figure 9. Future evolution of three-dimensional (3D) ultrastructural analysis of human biopsy samples

In focused-ion beam/scanning electron microscopy (FIB/SEM) tomography, the imaged

region of sample is completely lost due to FIB-milling (**Left panel**). Array tomography is a potential solution to this problem (**Right panel**). In this method, serial sectional SEM images are obtained from ultrathin serial sections mounted on a base. These ultrathin serial sections are physically stable and repeatedly observable.

REFERENCES

1. Kriz W, Kaissling B: Structural organization of the mammalian kidney. In: *The Kidney, Physiology and Pathophysiology.* 3rd ed. edited by Seldin DW, Giebisch G, Philadelphia, Lippincott Williams & Wilkins, 2000, pp 587-654.

2. Andrews PM: Scanning electron microscopy of human and rhesus monkey kidneys. *Lab Invest,* 32**:** 510-518, 1975.

3. Bulger RE, Siegel FL, Pendergrass R: Scanning and transmission electron microscopy of the rat kidney. *Am J Anat,* 139**:** 483-501, 1974.

4. Fujita T, Tokunaga J, Miyoshi M: Scanning electron microscopy of the podocytes of renal glomerulus. *Arch Histol Jpn,* 32**:** 99-113, 1970.

5. Ichimura K, Kakuta S, Kawasaki Y, Miyaki T, Nonami T, Miyazaki N, Nakao T, Enomoto S, Arai S, Koike M, Murata K, Sakai T: Morphological process of podocyte development revealed by block-face scanning electron microscopy. *J Cell Sci,* 130**:** 132-142, 2017.

6. Ichimura K, Miyazaki N, Sadayama S, Murata K, Koike M, Nakamura K, Ohta K, Sakai T: Three-dimensional architecture of podocytes revealed by block-face scanning electron microscopy. *Sci Rep,* 5**:** 8993, 2015.

7. Ichimura K, Sakai T: Evolutionary morphology of podocytes and primary urine-producing apparatus. *Anat Sci Int,* 92**:** 161-172, 2017.

8. Neal CR, Crook H, Bell E, Harper SJ, Bates DO: Three-dimensional reconstruction of glomeruli by electron microscopy reveals a distinct restrictive urinary subpodocyte space. *J Am Soc Nephrol,* 16**:** 1223-1235, 2005.

9. Takahashi-Iwanaga H: Comparative anatomy of the podocyte: A scanning electron microscopic study. *Microsc Res Tech,* 57**:** 196-202, 2002.

10. Neal CR: Podocytes ... What's Under Yours? (Podocytes and Foot Processes and How They Change in Nephropathy). *Front Endocrinol (Lausanne),* 6**:** 9, 2015.

11. Burghardt T, Hochapfel F, Salecker B, Meese C, Grone HJ, Rachel R, Wanner G, Krahn MP, Witzgall R: Advanced electron microscopic techniques provide a deeper

insight into the peculiar features of podocytes. *Am J Physiol Renal Physiol,* 309**:** F1082-1089, 2015.

12. Inokuchi S, Sakai T, Shirato I, Tomino Y, Koide H: Ultrastructural changes in glomerular epithelial cells in acute puromycin aminonucleoside nephrosis: a study by high-resolution scanning electron microscopy. *Virchows Arch A Pathol Anat Histopathol,* 423**:** 111-119, 1993.

13. Kriz W, Shirato I, Nagata M, LeHir M, Lemley KV: The podocyte's response to stress: the enigma of foot process effacement. *Am J Physiol Renal Physiol,* 304**:** F333-347, 2013.

14. Shirato I: Podocyte process effacement in vivo. *Microsc Res Tech,* 57**:** 241-246, 2002.

15. Inokuchi S, Shirato I, Kobayashi N, Koide H, Tomino Y, Sakai T: Re-evaluation of foot process effacement in acute puromycin aminonucleoside nephrosis. *Kidney Int,* 50**:** 1278-1287, 1996.

16. Dong HM, Ichimura K, Sakai T: Structural organization of hepatic portal vein in rat with special reference to musculature, intimal folds, and endothelial cell alignment. *Anat Rec (Hoboken),* 293**:** 1887-1895, 2010.

17. Caulfield JP, Reid JJ, Farquhar MG: Alterations of the glomerular epithelium in acute aminonucleoside nephrosis. Evidence for formation of occluding junctions and epithelial cell detachment. *Lab Invest,* 34**:** 43-59, 1976.

18. Kanwar YS, Rosenzweig LJ: Altered glomerular permeability as a result of focal detachment of the visceral epithelium. *Kidney Int,* 21**:** 565-574, 1982.

19. Messina A, Davies DJ, Dillane PC, Ryan GB: Glomerular epithelial abnormalities associated with the onset of proteinuria in aminonucleoside nephrosis. *Am J Pathol,* 126**:** 220-229, 1987.

20. Ryan GB, Karnovsky MJ: An ultrastructural study of the mechanisms of proteinuria in aminonucleoside nephrosis. *Kidney Int,* 8**:** 219-232, 1975.

21. Venkatachalam MA, Karnovsky MJ, Cotran RS: Glomerular permeability. Ultrastructural studies in experimental nephrosis using horseradish peroxidase as a

tracer. *J Exp Med,* 130**:** 381-399, 1969.

22. Ribeiro C, Neumann M, Affolter M: Genetic control of cell intercalation during tracheal morphogenesis in Drosophila. *Curr Biol,* 14**:** 2197-2207, 2004.

23. Rasch R, Nyengaard JR, Marcussen N, Meyer TW: Renal structural abnormalities following recovery from acute puromycin nephrosis. *Kidney Int,* 62**:** 496-506, 2002.

24. Uchida K, Suzuki K, Iwamoto M, Kawachi H, Ohno M, Horita S, Nitta K: Decreased tyrosine phosphorylation of nephrin in rat and human nephrosis. *Kidney Int,* 73**:** 926-932, 2008.

25. Yaoita E, Yao J, Yoshida Y, Morioka T, Nameta M, Takata T, Kamiie J, Fujinaka H, Oite T, Yamamoto T: Up-regulation of connexin43 in glomerular podocytes in response to injury. *Am J Pathol,* 161**:** 1597-1606, 2002.

26. Kriz W, Lemley KV: A potential role for mechanical forces in the detachment of podocytes and the progression of CKD. *J Am Soc Nephrol,* 26**:** 258-269, 2015.

27. Kriz W, Hahnel B, Hosser H, Rosener S, Waldherr R: Structural analysis of how podocytes detach from the glomerular basement membrane under hypertrophic stress. *Front Endocrinol (Lausanne),* 5**:** 207, 2014.

28. Micheva KD, Smith SJ: Array tomography: a new tool for imaging the molecular architecture and ultrastructure of neural circuits. *Neuron,* 55**:** 25-36, 2007.

29. Wacker I, Schroeder RR: Array tomography. *J Microsc,* 252**:** 93-99, 2013.

30. Koga D, Kusumi S, Watanabe T: Backscattered electron imaging of resin-embedded sections. *Microscopy (Oxf)*, 2018.

31. Koike T, Kataoka Y, Maeda M, Hasebe Y, Yamaguchi Y, Suga M, Saito A, Yamada H: A device for ribbon collection for array tomography with scanning electron microscopy. *Acta Histochem Cytochem,* 50**:** 135-140, 2017.

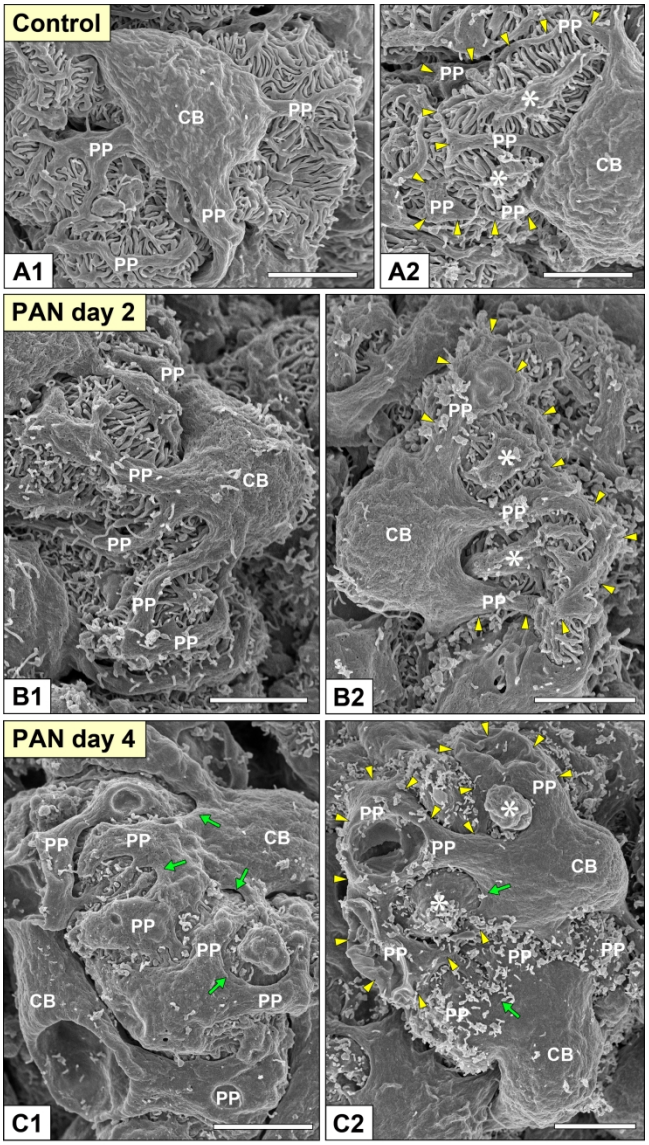

Figure 1
Ichimura et al.

205x382mm (300 x 300 DPI)

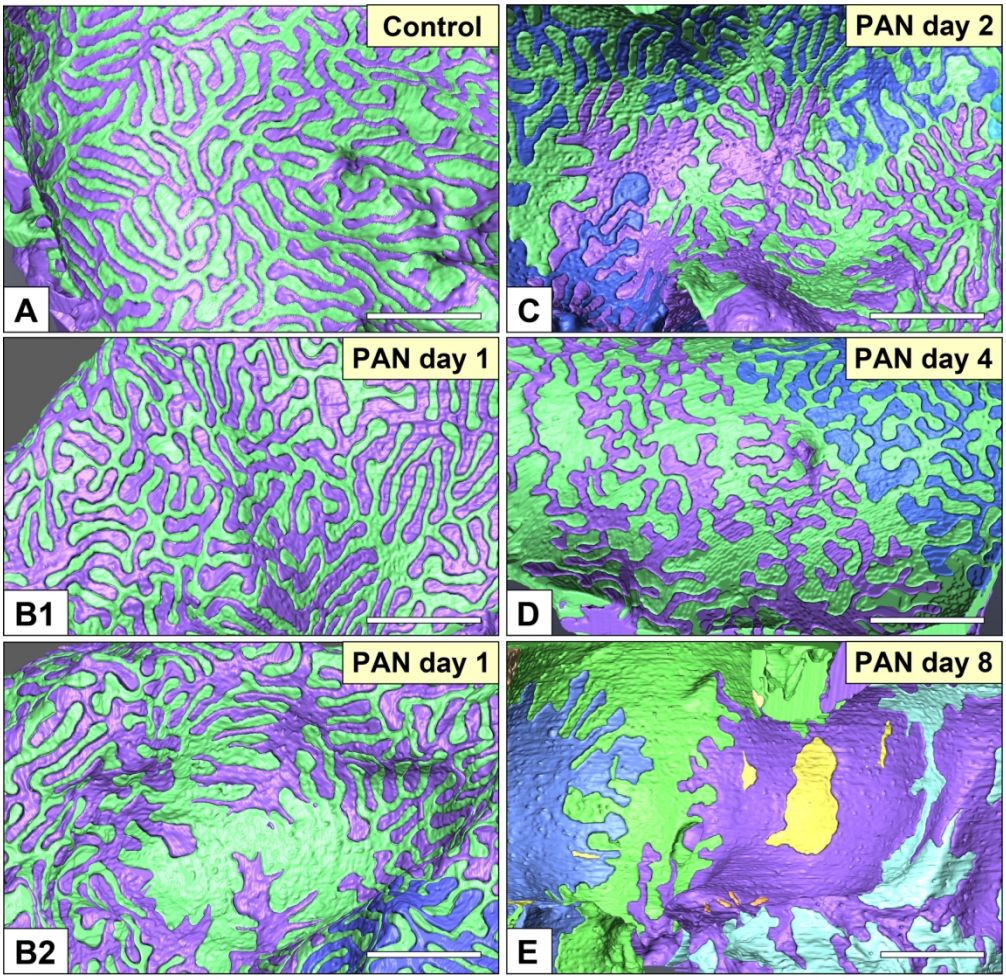

Figure 2
Ichimura et al.

157x165mm (300 x 300 DPI)

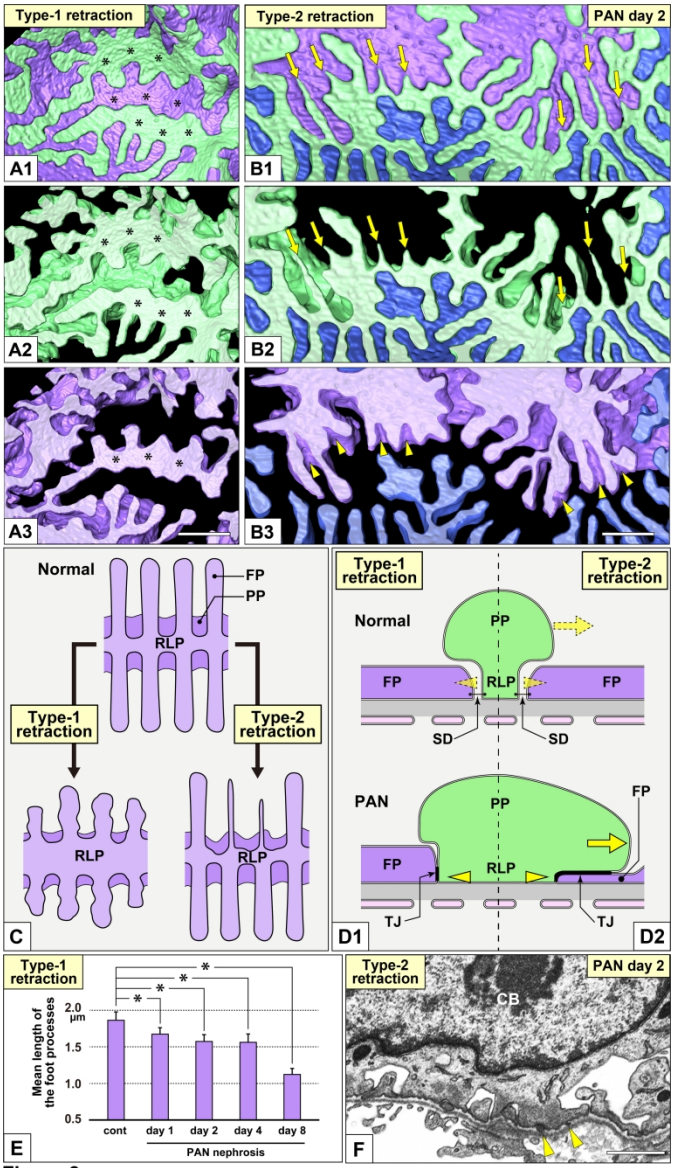

Figure 3
Ichimura et al.

255x457mm (300 x 300 DPI)

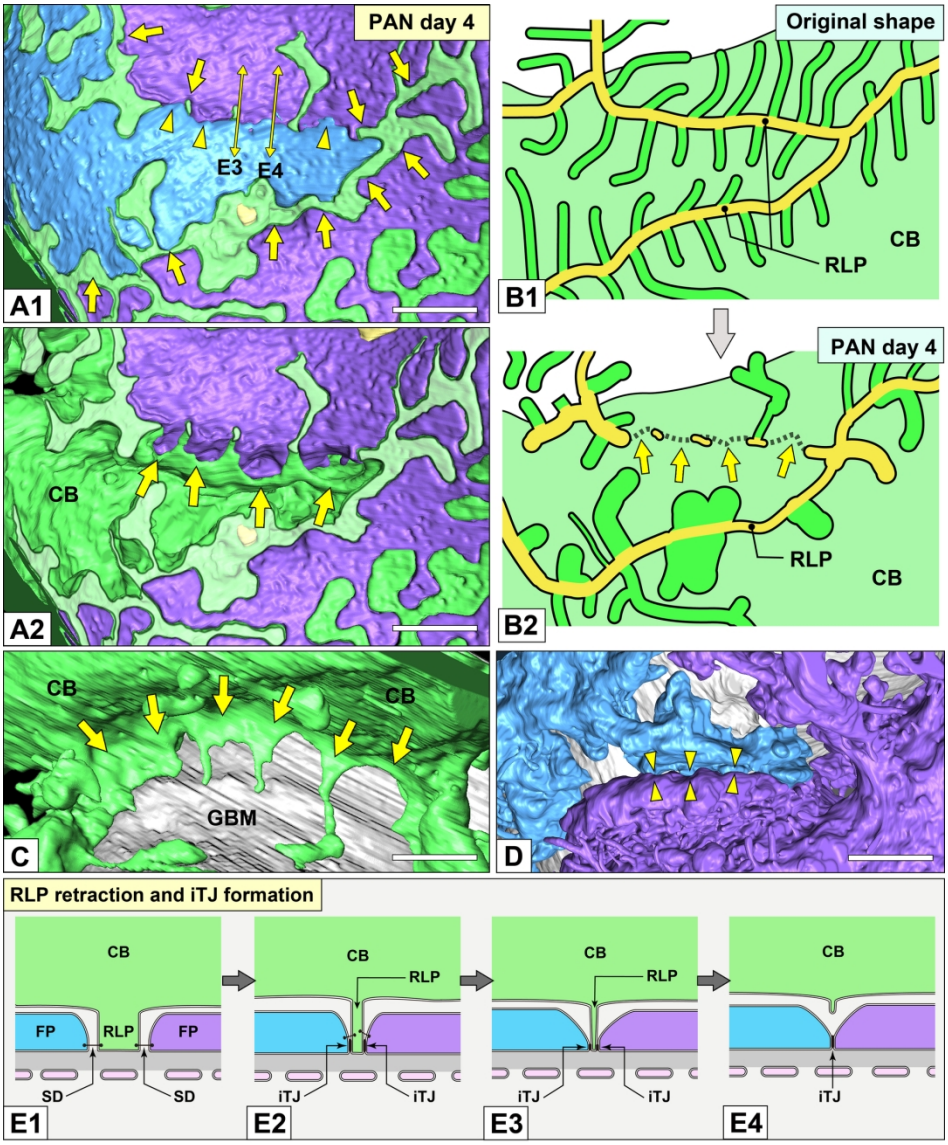

Figure 4
Ichimura et al.

170x216mm (300 x 300 DPI)

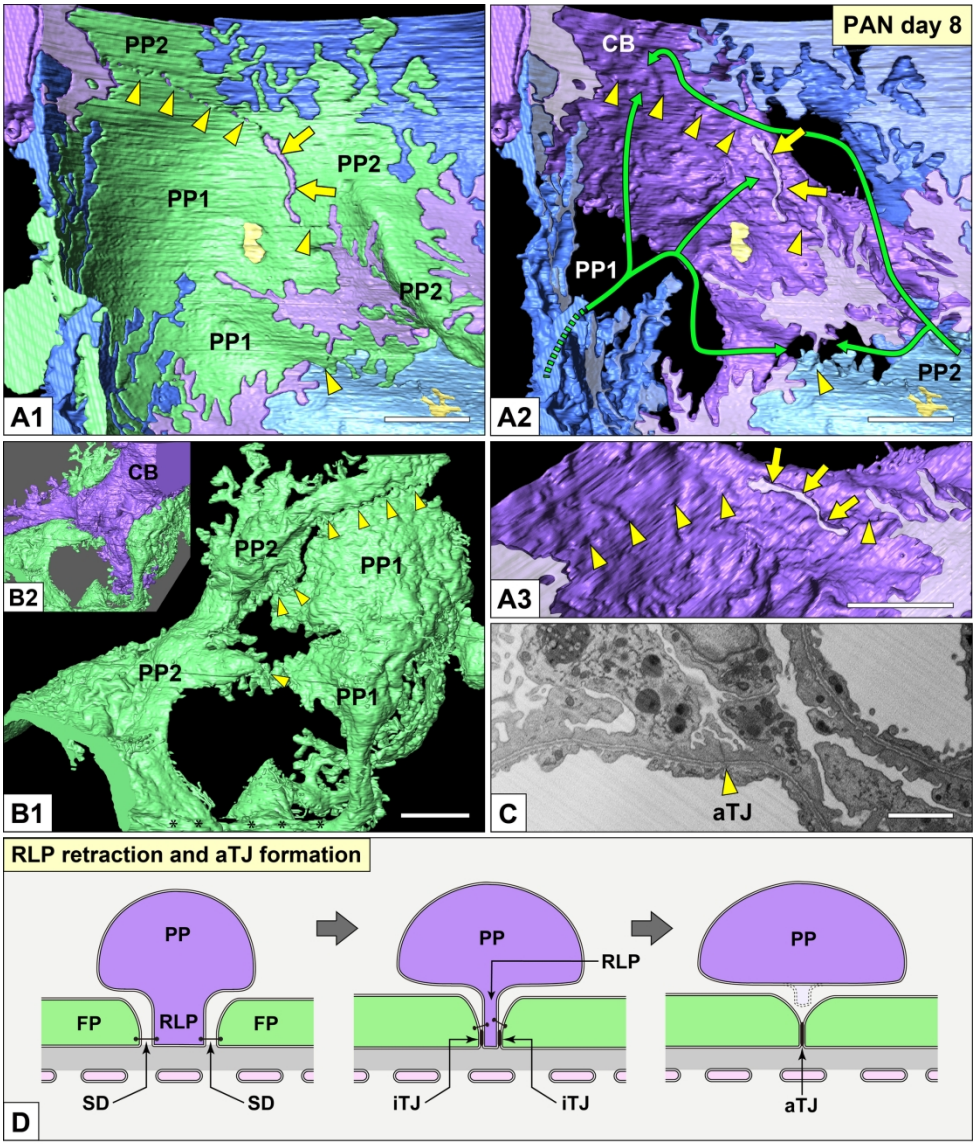

Figure 5
Ichimura et al.

210x259mm (300 x 300 DPI)

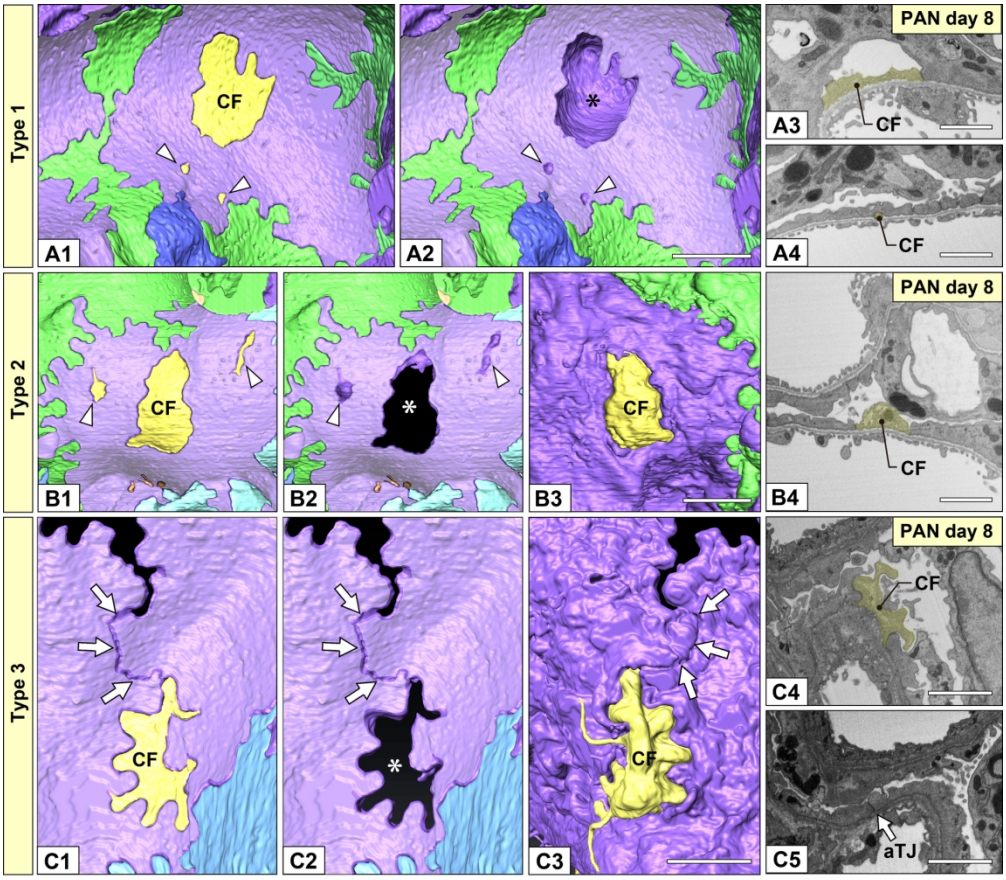

Figure 6
Ichimura et al.

168x157mm (300 x 300 DPI)

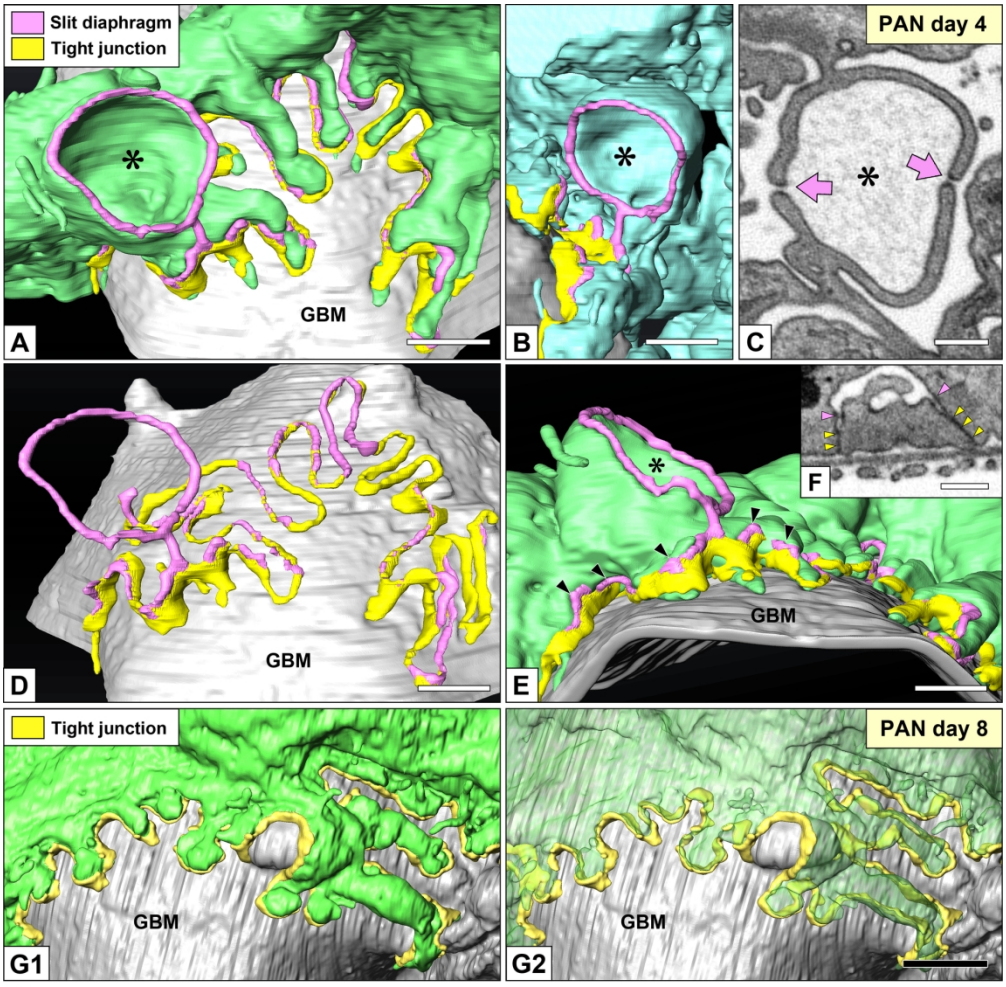

Figure 7
Ichimura et al.

168x175mm (300 x 300 DPI)

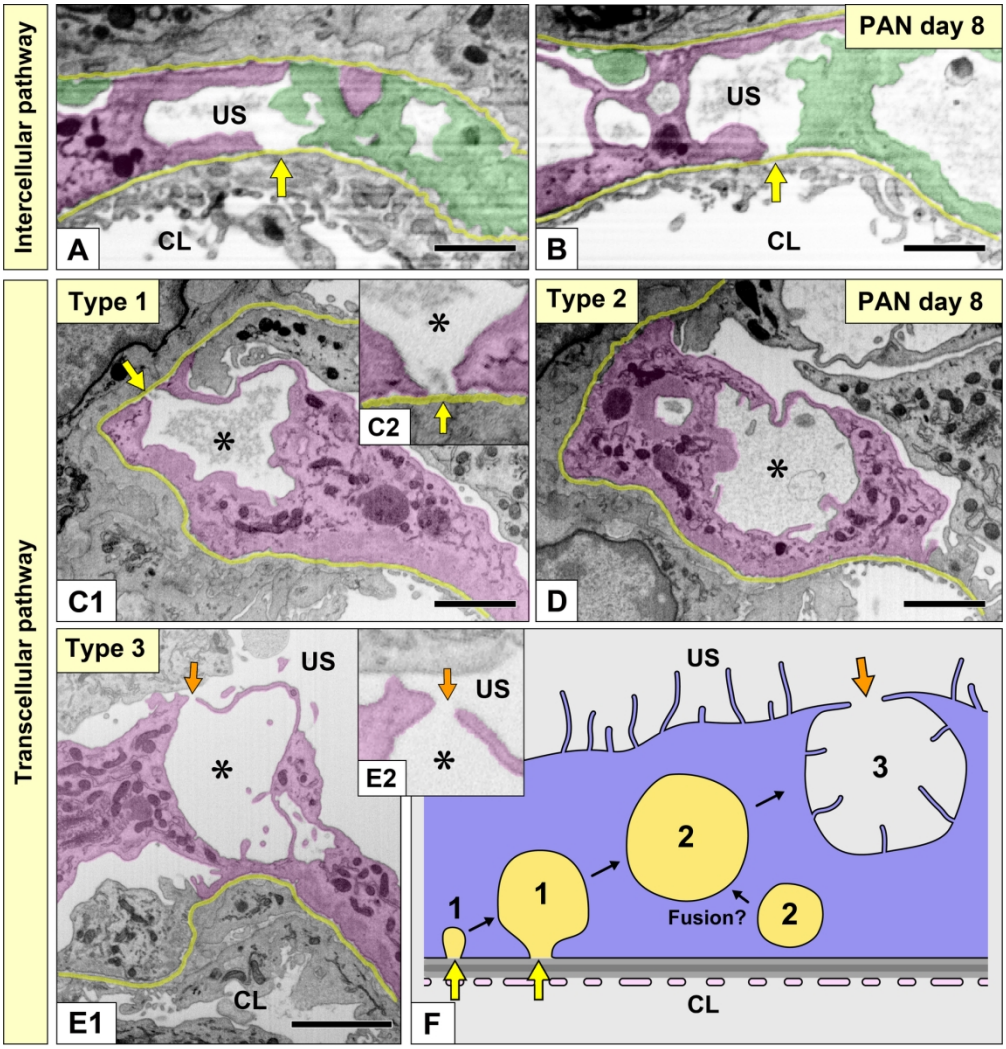

Figure 8
Ichimura et al.

166x184mm (300 x 300 DPI)

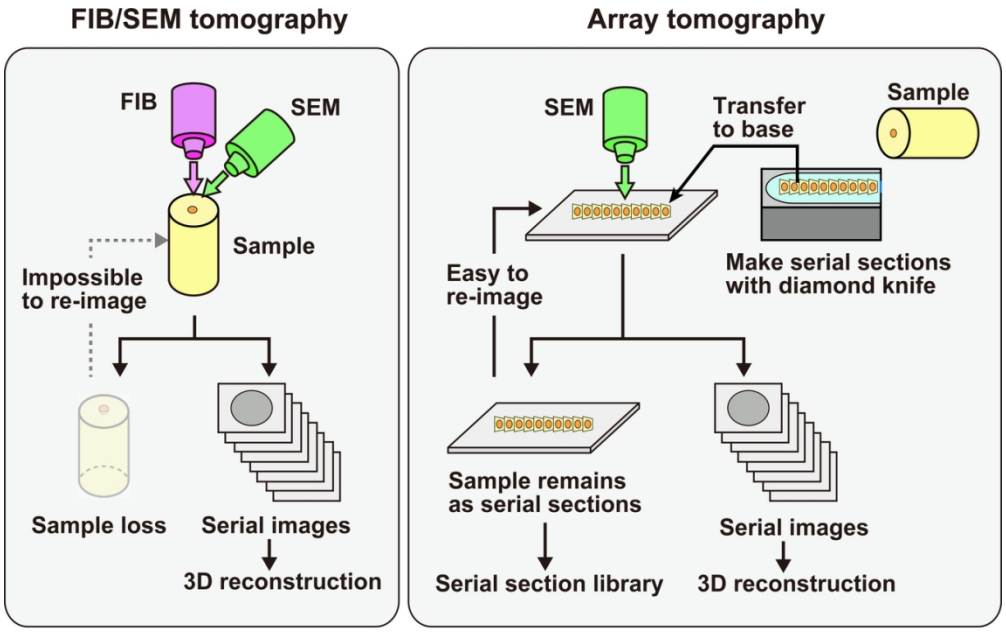

Figure 9
Ichimura et al.

115x79mm (300 x 300 DPI)

SUPPLEMENTARY INFORMATION

Morphological Processes of Foot Process Effacement in Puromycin Aminonucleoside Nephrosis Revealed by FIB/SEM Tomography

Koichiro Ichimura[1,2], Takayuki Miyaki[1], Yuto Kawasaki[1], Mui Kinoshita[1], Soichiro Kakuta[2], and Tatsuo Sakai[1]

[1]Department of Anatomy and Life Structure, Juntendo University Graduate School of Medicine, Tokyo, Japan; [2]Laboratory of Morphology and Image Analysis, Research Support Center, Juntendo University Graduate School of Medicine, Tokyo, Japan.

Table of Contents:

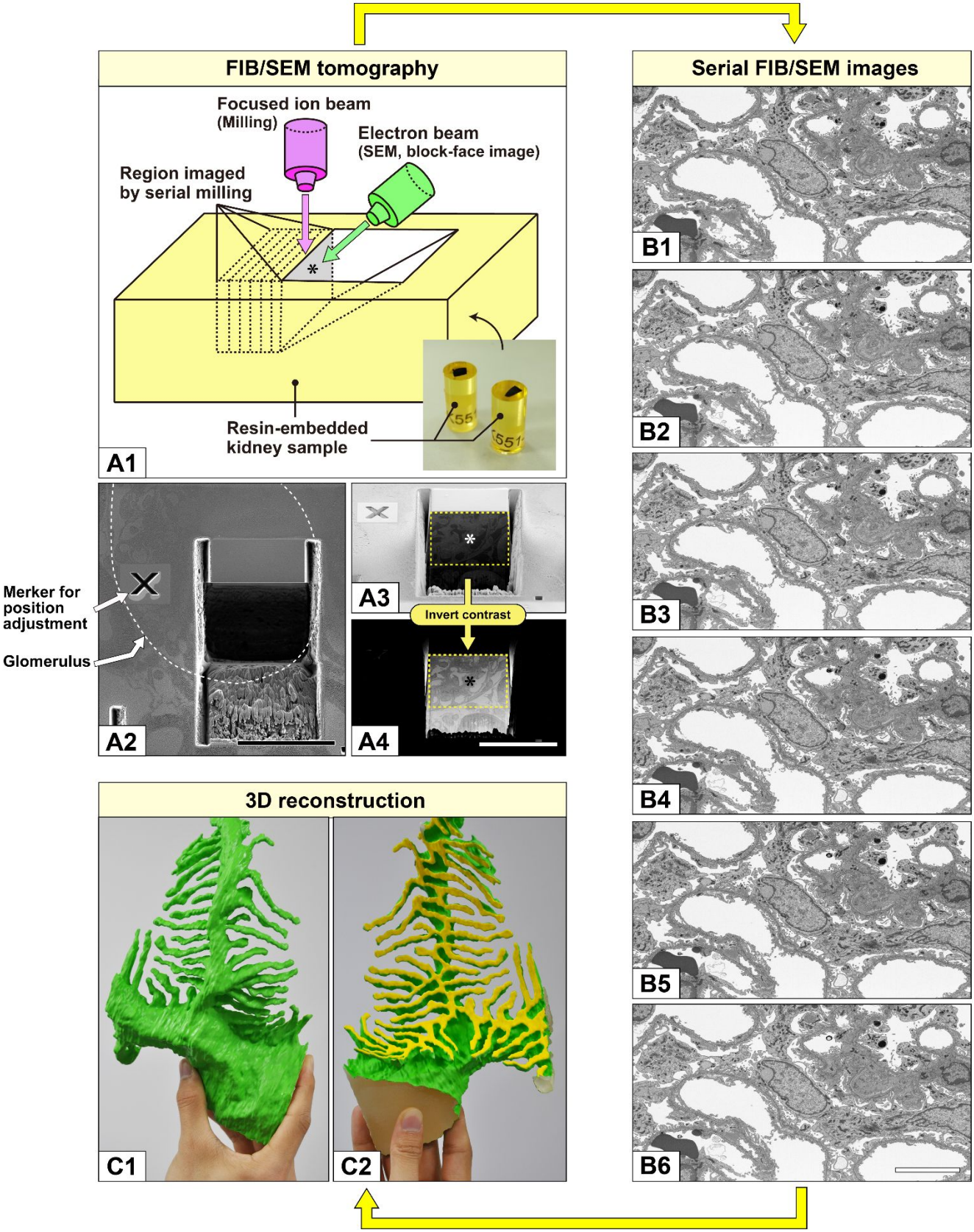

Supplementary Figure 1. 3D reconstruction of podocytes using focused-ion beam/scanning electron microscopy (FIB/SEM) tomography.

(**A1**–**4**) Image acquisition in FIB/SEM tomography. (**A1**) Schematic drawing of the positional relationships of the resin-embedded sample (yellow), FIB column (pink), and SEM column (green). The cross-sectional surface, which is called the “block face” (asterisk), was generated using FIB milling. The block face was perpendicular to the surface of the sample. The SEM column was placed obliquely to scan the block face. (**A2**) The sample surface observed perpendicular to the block face. (**A3** and **A4**) To image the block face (asterisks), the sample was observed obliquely as shown in **A1**. The imaged region is indicated by a yellow rectangle. The contrast-inverted FIB/SEM image is quite similar to a conventional transmission electron microscopy (TEM) image of an ultrathin section. (**B1**–**6**) Serial FIB/SEM images. The generation of the cross-sectional surface using FIB milling and SEM imaging were serially and automatically performed to acquire serial FIB/SEM images. (**C1** and **C2**) 3D reconstruction. Reconstructed image of a single podocyte was produced from the serial FIB/SEM images using an AMIRA 6.1 reconstruction software. It was then printed using a ProJet HD3500Plus 3D printer for detailed analysis and presentation. Scale bars: 50 μm in **A2** and **A4**; 5 μm in **B6**.

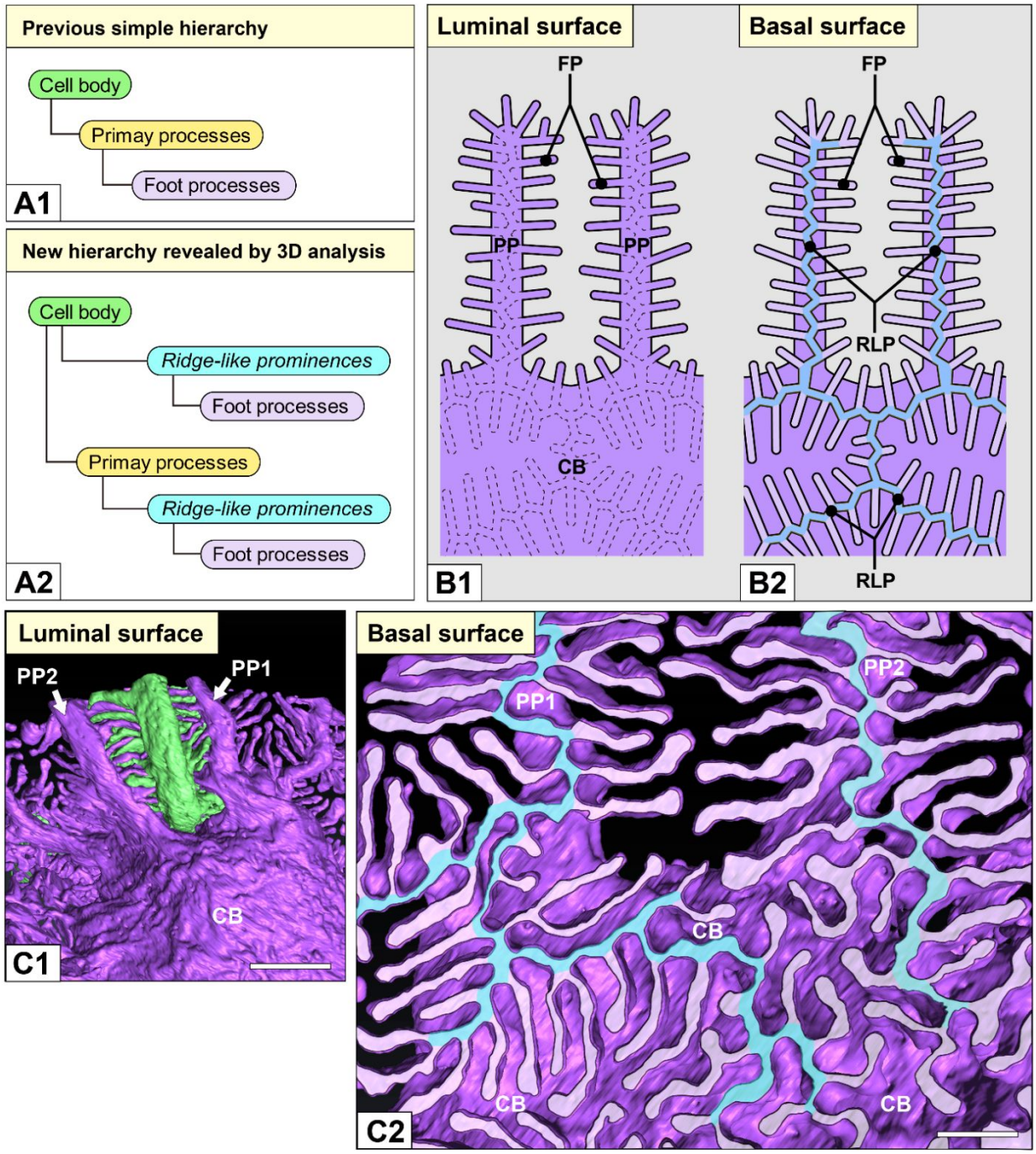

Supplementary Figure 2. Structural hierarchy of podocyte subcellular compartments. (**A1**) Previous simple hierarchy. The three subcellular compartments of the podocyte—cell body, primary processes, and foot processes—are related in this order. (**A2**) New hierarchy based on our previous 3D analysis. The ridge-like prominences (RLPs), which protrude from the basal surface of the cell body and primary processes, serve as an adhesion apparatus for the attachment of the cell body and primary processes to the GBM and to connect foot processes to the cell body and primary processes. (**B1** and **B2**) Schematic representation of podocyte subcellular compartments based on the new hierarchy. RLPs are colored blue (**B2**). The RLPs under the cell body are subject to variation and not as regular as under the primary processes. (**C1** and **C2**) 3D reconstruction of podocytes.

The luminal and basal surfaces of the same purple podocyte are shown. RLPs are colored blue in **C2**. CB, cell body; FP, foot process; PP, primary process. Scale bars: 2 μm in **C1**; 500 nm in **C2**.

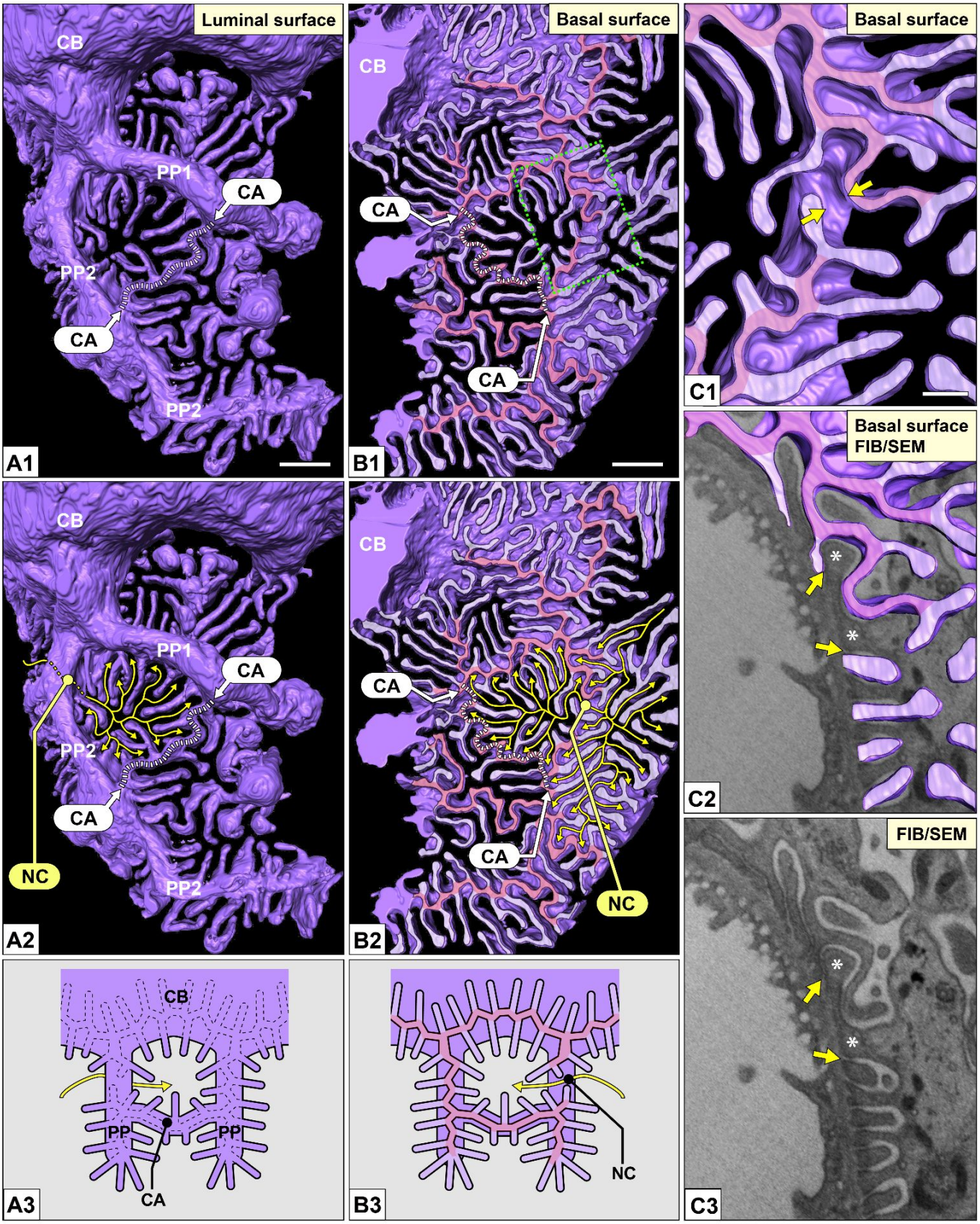

Supplementary Figure 3. Cytoplasmic arcade (CA) in normal podocyte (I).
Luminal (**A1**–**3**) and basal (**B1**–**3**) views of single reconstructed podocyte. (**A1**) The CA (dotted lines) is an anastomosis between two parental primary processes (PP1 and PP2), which are derived from the same cell body (CB). (**B1**) Ridge-like prominences (RLPs) are colored pink. Similar to primary processes, the CA (dotted lines) also possesses RLP and foot processes. (**A2** and **B2**) Neighboring podocyte (yellow line) entered the space surrounded by PP1, PP2, and CA via a narrow channel (NC) under PP2. The dotted lines in **A2** and **B2** represent the CA and its RLP, respectively. (**A3** and **B3**) Schematic representation of CA. (**C1**–**3**) Magnification of NC and its corresponding focused-ion beam/scanning electron microscopy (FIB/SEM) image. The slit diaphragms (arrows in **C2** and **C3**) were formed between the purple podocyte and the neighboring podocyte passing this NC (arrows in **C1**). Asterisks, the neighboring podocyte passing through the NC. Scale bars: 1 μm in **A1** and **B1**; 500 nm in **C1**.

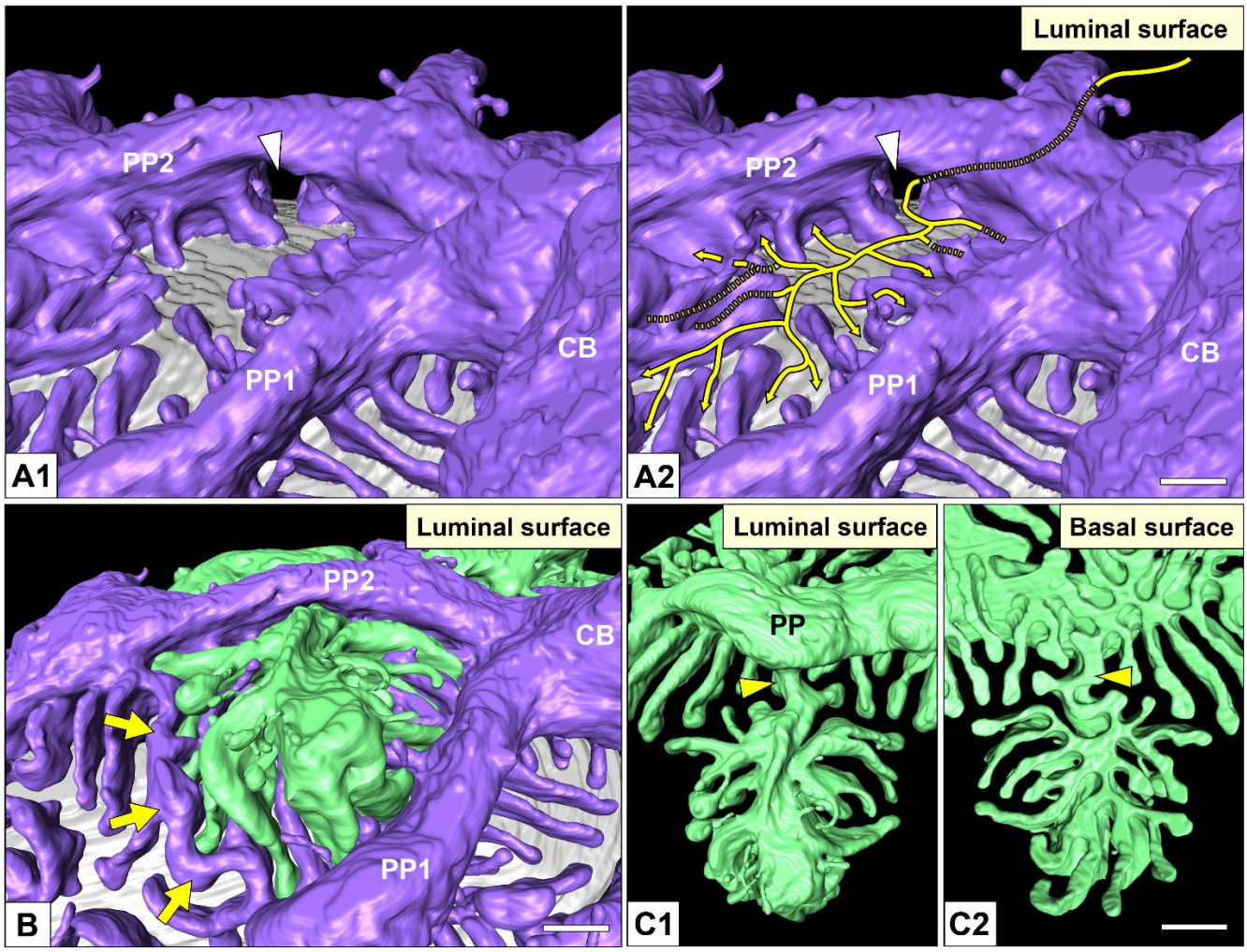

Supplementary Figure 4. Cytoplasmic arcade (CA) in normal podocyte (II).
Purple podocyte is the same cell shown in **Supplementary Figure 3**. (**A1** and **A2**) Luminal view. The narrow channel (NC, arrowheads) is surrounded by the primary process, ridge-like prominences (RLPs), and glomerular basement membrane (GBM, gray). Yellow line in **A2** represents neighboring podocyte passing through the NC. (**B**) Luminal view. Green podocyte, which is shown by the yellow lines in **Supplementary Figures 3A2**, **3B2**, **4A2**, passes through the NC and enters the space surrounded by the CA (arrows) and its parental primary processes (PP1, PP2). (**C1** and **C2**) Magnification of the green podocyte shown in **B**. Arrowheads indicate the part passing through the NC of the purple podocyte. CB, cell body; PP, primary process. Scale bars: 500 nm in **A2**, **B**, and **C2**.

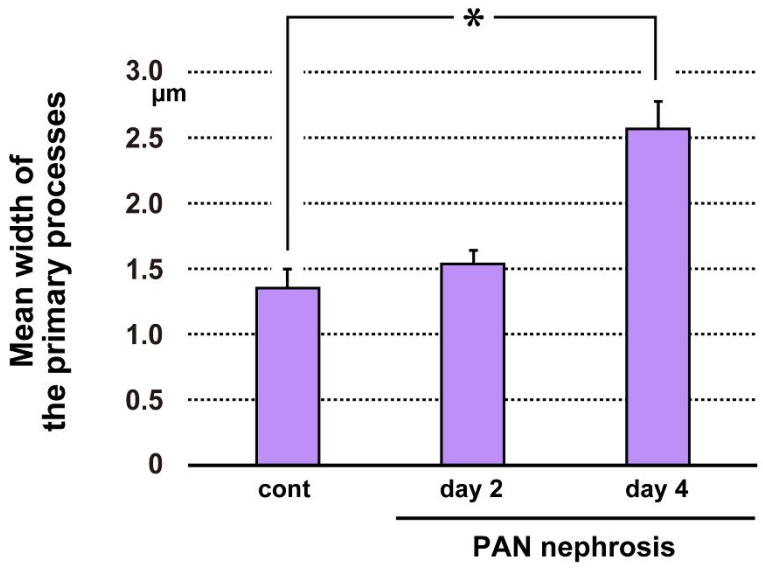

Supplementary Figure 5. Alteration in mean width of primary processes in PAN nephrotic podocytes. The width was measured immediately after primary processes protruded from the cell body on the conventional scanning electron microscopy (SEM) images. The mean width significantly increased on day 4 (overt proteinuria phase) compared with control: control, 1.35 ± 0.14 μm; day 2, 1.54 ± 0.11 μm; day 4, 2.57 ± 0.21 μm (n = 40 primary processes from six to eight podocytes). Values are means ± standard error of the mean. Differences were tested using ANOVA followed by the Bonferroni test as post hoc test. *$P < 0.05$.

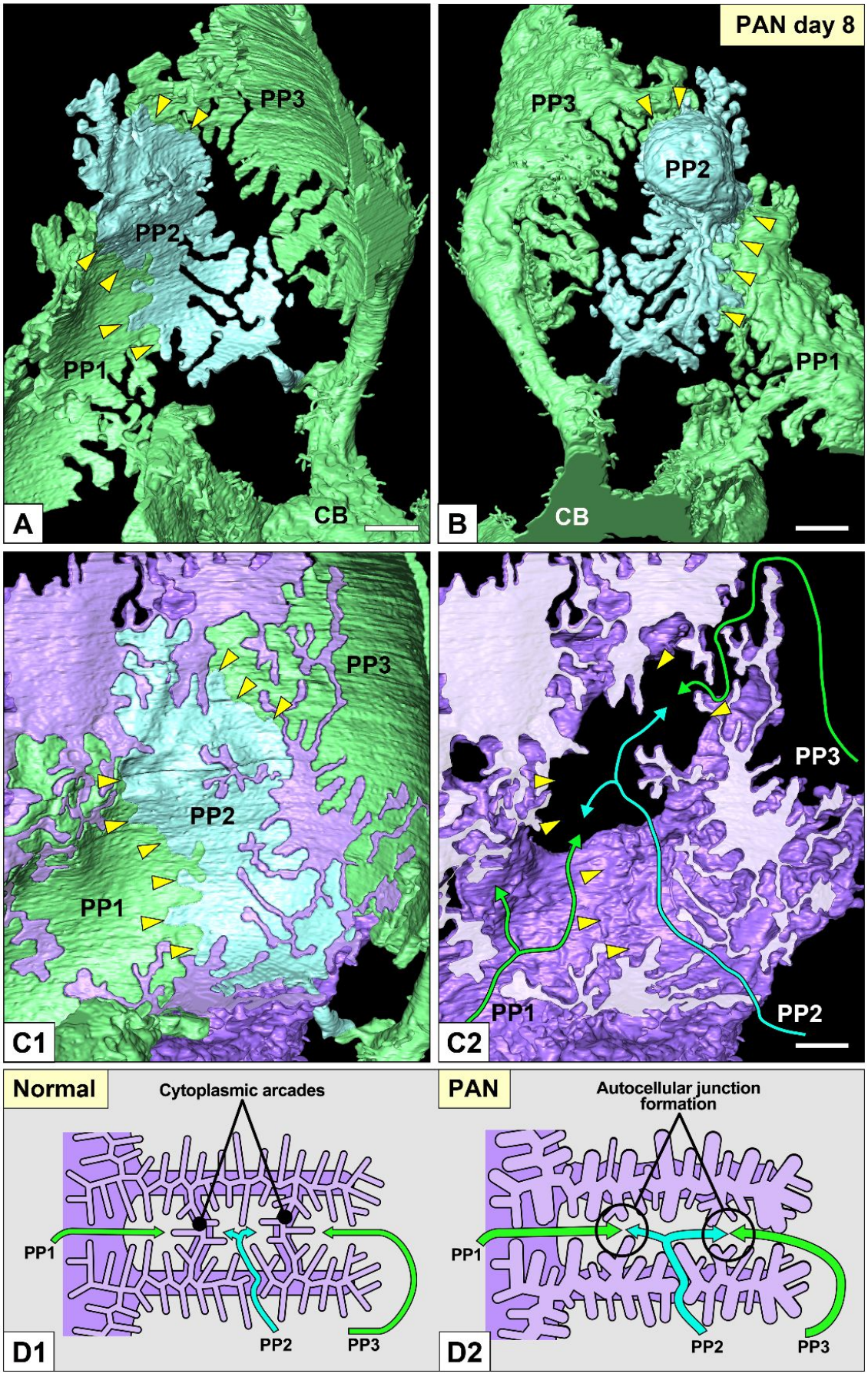
PAN day 8
PP3
PP2
PP1
CB
A
B
C1
C2
Normal
Cytoplasmic arcades
PAN
Autocellular junction formation
D1
D2

Supplementary Figure 6. Formation of autocellular tight junctions in PAN nephrotic podocytes. Disappearance of cytoplasmic arcades (CAs) is related to formation of aTJ. (**A**, **C1**, **C2**, **D1**, and **D2**) Basal view. (**B**) Luminal view. (**A** and **B**) Three deformed primary processes (PP1, PP2, and PP3) were derived from the same cell body (CB). Two aTJs formed between PP1 and PP2 and between PP2 and PP3 (arrowheads). (**C1** and **C2**) CAs and their ridge-like prominences (RLPs) of the purple podocyte were presumably situated at the positions of aTJs (arrowheads). Disappearance of CAs allowed the formation of aTJs in green podocyte. (**C2**) PP1–3 were removed from **C1**, and the positions of PP1–3 are indicated by the green and blue lines. (**D1** and **D2**) Schematic representations of the aTJ formation by CA disappearance in the purple podocyte. Scale bars: 500 nm in **A**, **B**, and **C2**.

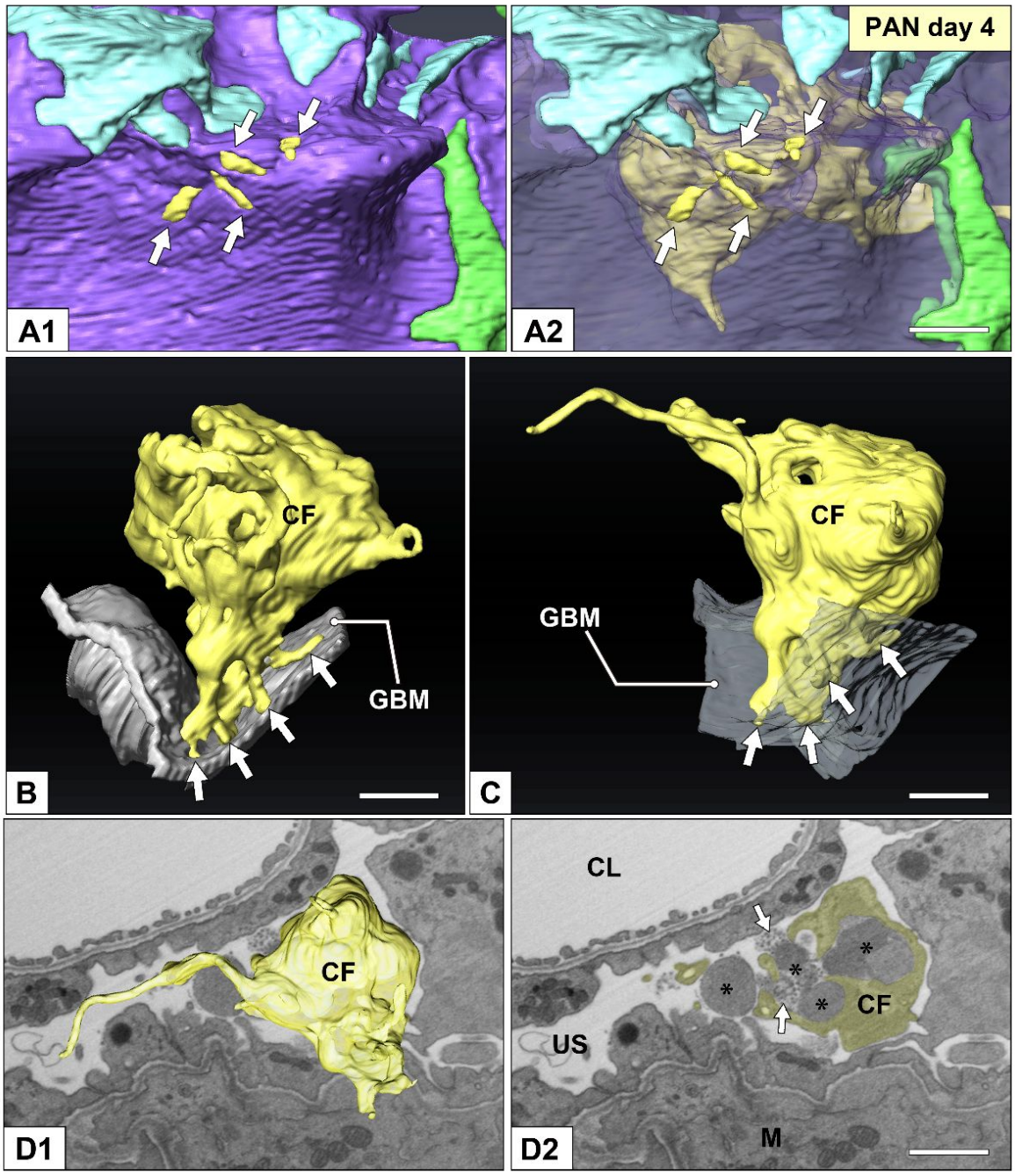

Supplementary Figure 7. Shedding cytoplasmic fragment (CF) in PAN nephrotic podocytes. (**A1** and **A2**) Basal view. Yellow represents shedding CF, which exhibited considerably narrow attachment sites to the glomerular basement membrane (GBM) (arrows). Neighboring purple podocyte turned translucent in **A2**. (**B** and **C**) Isolated yellow CF with the GBM, which turned translucent in **C**. (**D1** and **D2**) Focused-ion beam/scanning electron microscopy (FIB/SEM) images of the shedding CF. The shedding CF exhibit necrotizing alterations and the release of the contents of lysosomes (asterisks in **D2**) and multivesicular bodies (arrows in **D2**) into the urinary space (US). CL, capillary lumen; M, mesangium. Scale bars: 500 nm in **A**, **B**, and **C2**.

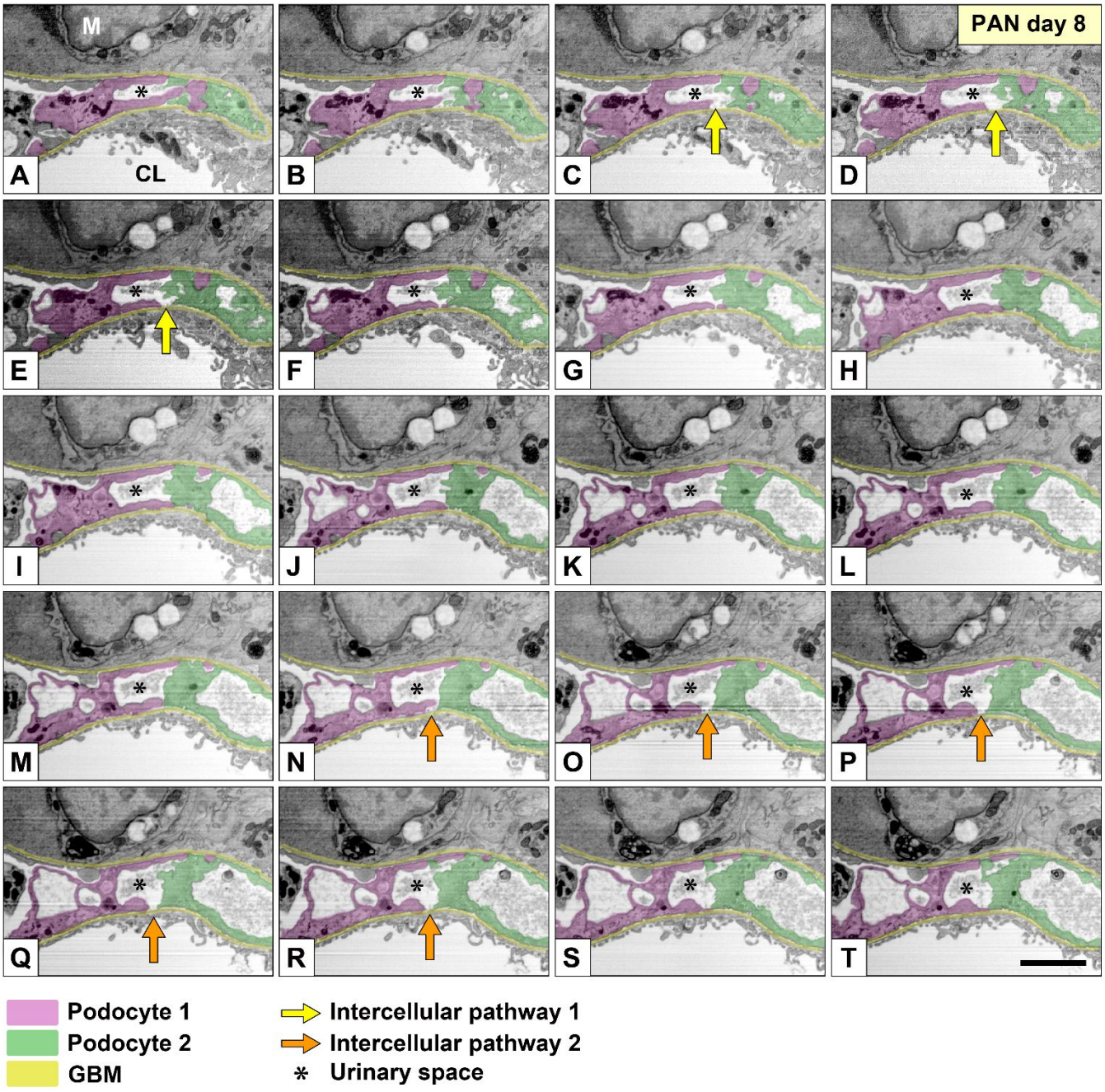

Supplementary Figure 8. Intercellular pathways for plasma protein leakage shown by serial focused-ion beam/scanning electron microscopy (FIB/SEM) images.

The intercellular pathway consists of the intercellular gaps without junctional structures (slit diaphragm and tight junction) between deformed podocytes and the microdenudation of glomerular basement membrane (GBM) at the intercellular gaps. These FIB/SEM images, selected after every four images from the complete original serial FIB/SEM images, contained two intercellular pathways/gaps end to end. Intercellular pathways/gaps between green and purple podocytes are indicated by yellow arrows (**B**–**E**) and orange arrows (**N**–**R**). GBM is colored in yellow. CL, capillary lumen; M, mesangium; asterisks, urinary space. Scale bar: 200 nm.

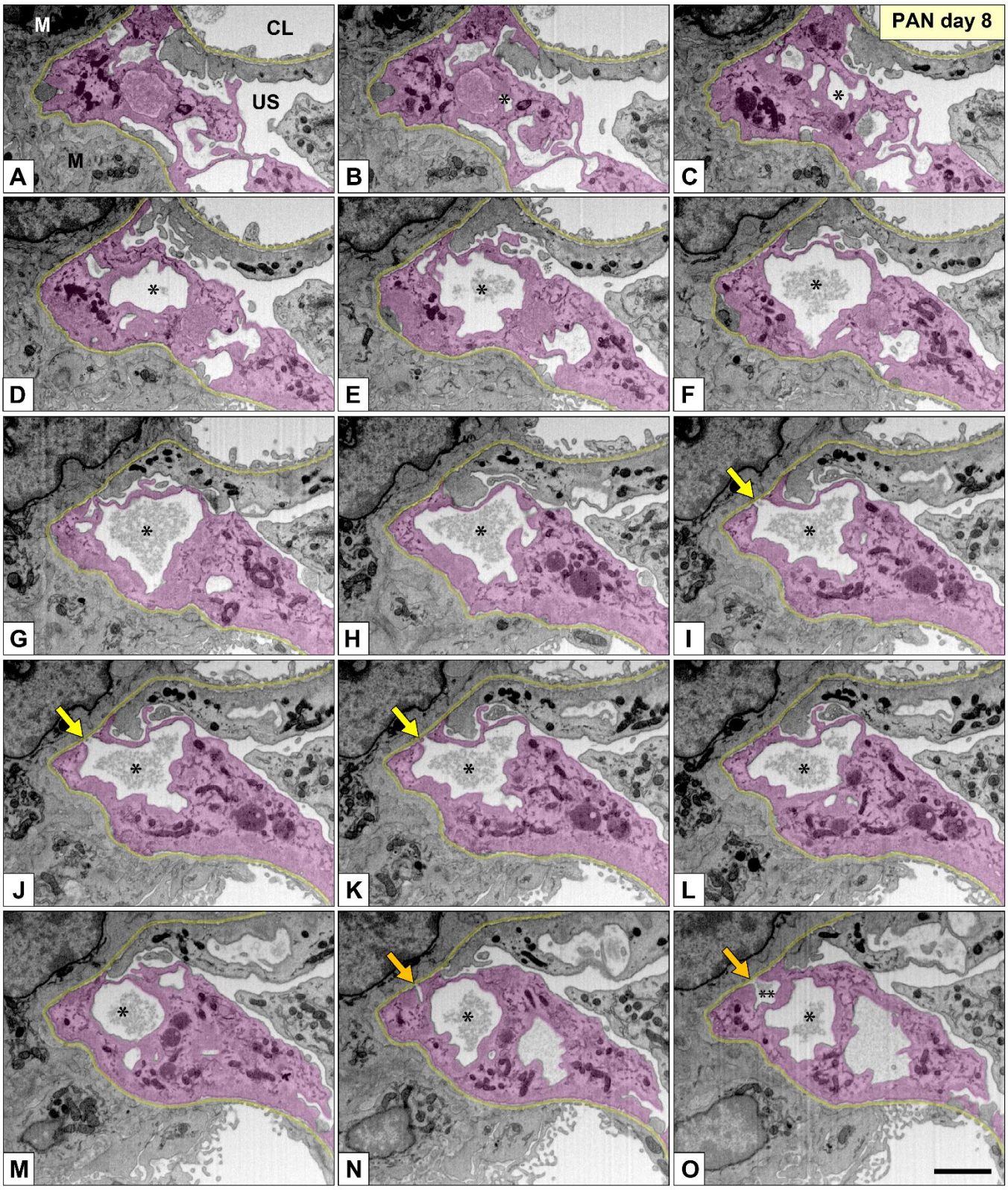

Continued on the next page.

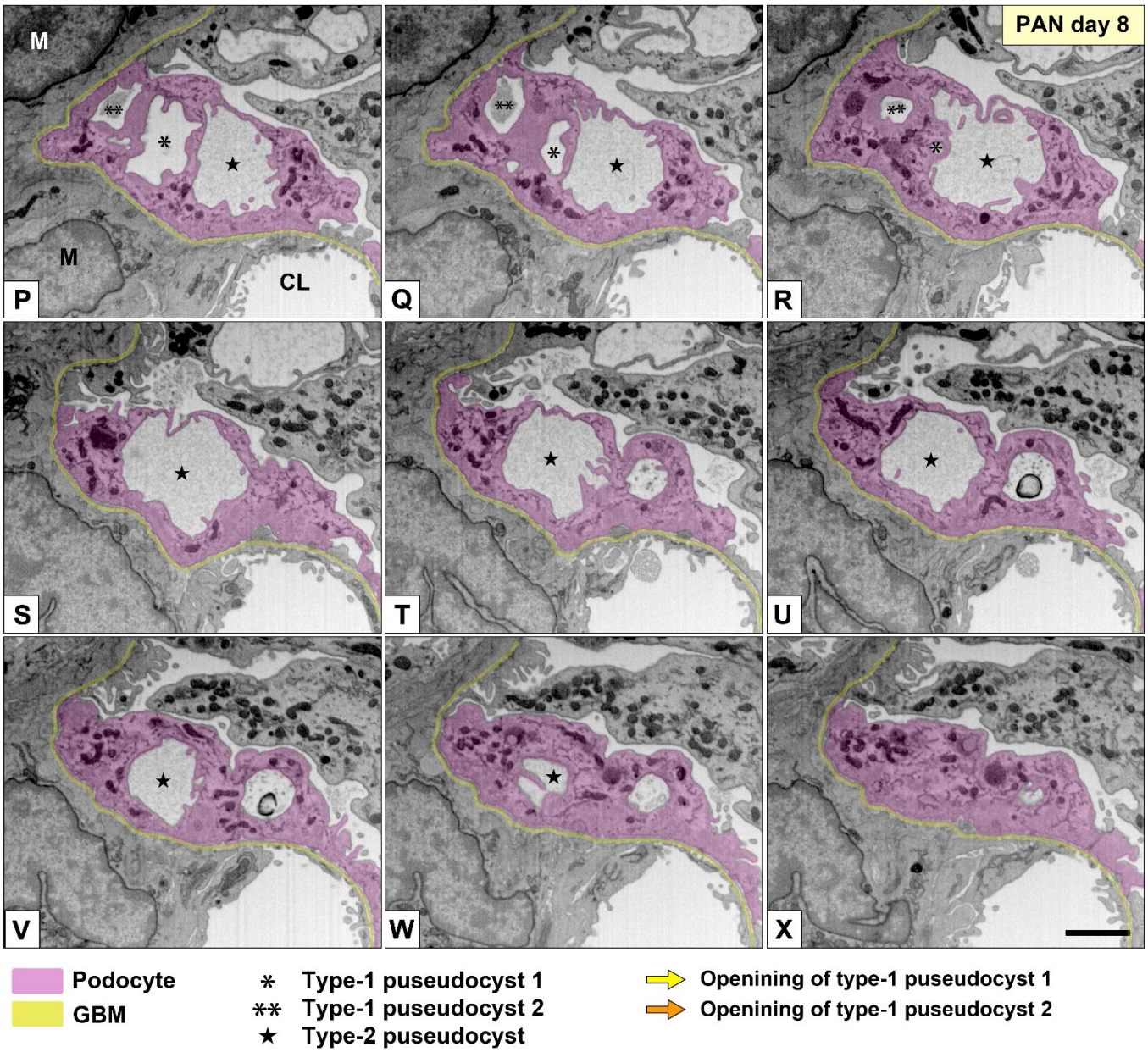

Supplementary Figure 9. Types-1 and -2 pseudocysts shown by serial focused-ion beam/scanning electron microscopy (FIB/SEM) images.

Type-1 pseudocysts are dome-shaped and outpocketing structures that develop in conjunction with focal microdenudation of the glomerular basement membrane (GBM); type-2 pseudocysts are completely closed. These FIB/SEM images, selected after every five images from the complete original serial FIB/SEM images, contained two type-1 pseudocysts (asterisks in **B**–**R** and double asterisks in **N**–**R**) and one type-2 pseudocyst (stars in **M**–**W**) end to end. These pseudocysts are formed within the purple podocyte. The openings of type-1 pseudocysts are indicated by yellow arrows (**I**–**K**) and orange arrows (**N** and **O**). Types-1 and -2 pseudocysts contain amorphous materials, which are reminiscent of the plasma protein aggregation due to the chemical fixation. GBM is colored in yellow. CL, capillary lumen; M, mesangium; US, urinary space. Scale bar: 500 nm.

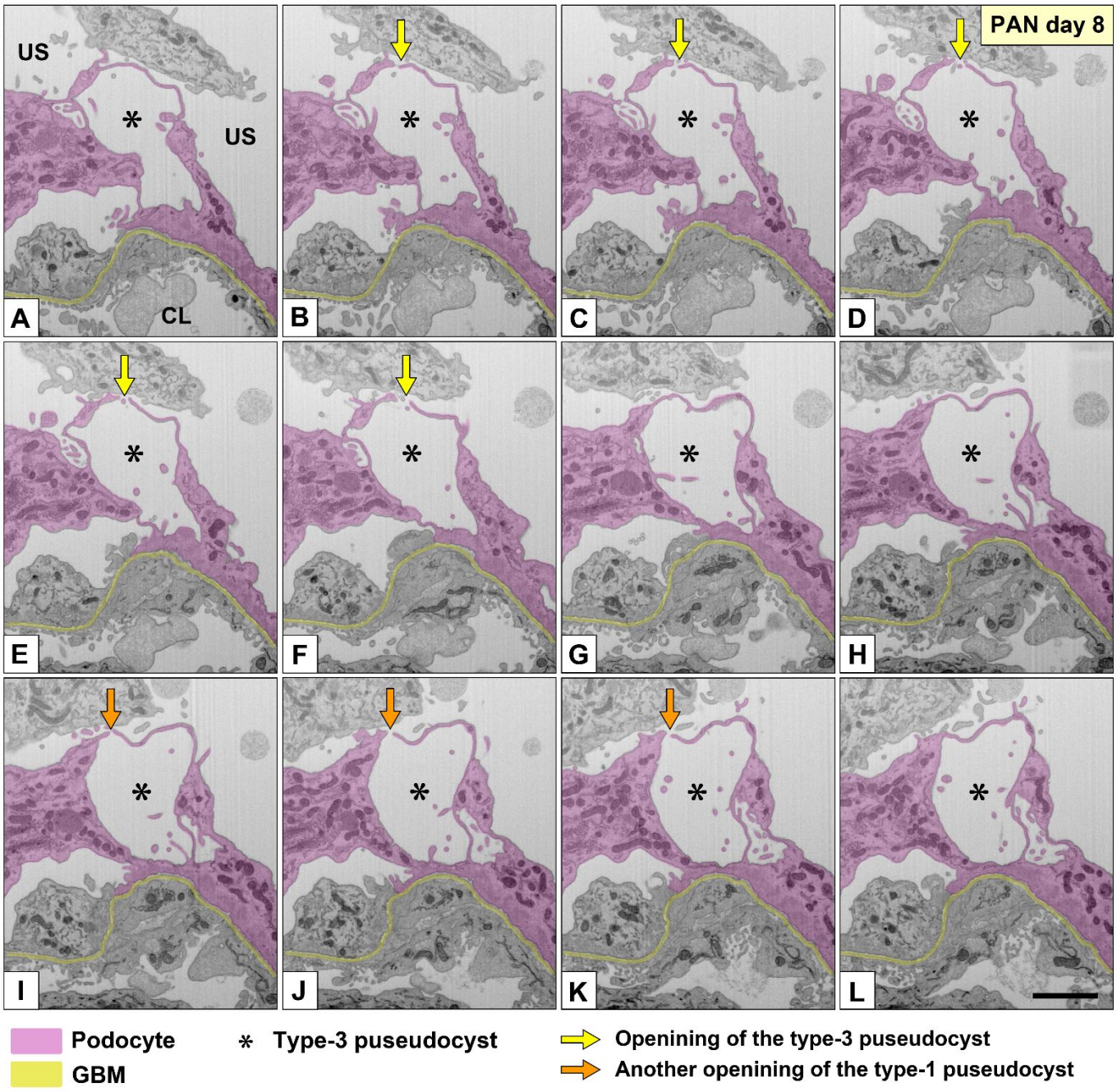

Supplementary Figure 10. Type-3 pseudocyst shown by serial focused-ion beam/scanning electron microscopy (FIB/SEM) images.

Type-3 pseudocyst are opened to the urinary space through small channels. These FIB/SEM images, selected every five images from the complete original serial FIB/SEM images, contained two small channels (arrows in **B**–**F** and **I**–**K**) of the type-1 pseudocyst end to end. These pseudocysts are formed within the purple podocyte. Type-3 pseudocysts do not contain amorphous materials. Asterisks indicate the lumen of type-3 pseudocyst. GBM is colored in yellow. CL, capillary lumen; US, urinary space. Scale bar: 500 nm.

SIGNIFICANCE STATEMENT

Although foot process effacement is a known pathological marker of podocyte injury, its morphological development has not been elucidated. To clarify the 3D morphology during foot process effacement, we analyzed reconstructed puromycin nephrotic podocytes made from serial, sectional focused-ion beam/scanning electron microscopy (FIB/SEM) images. The high-quality 3D reconstructed images enabled the successful description of the 3D morphological changes during foot process effacement and its associated alterations such as fragmentation, autocellular tight junctions, and ridge-like prominence retraction, in greater detail than has been described based on conventional electron microscopy.

Journal of the American Society of NEPHROLOGY

Morphological processes of foot process effacement in PAN nephrosis revealed by FIB/SEM tomography

Method

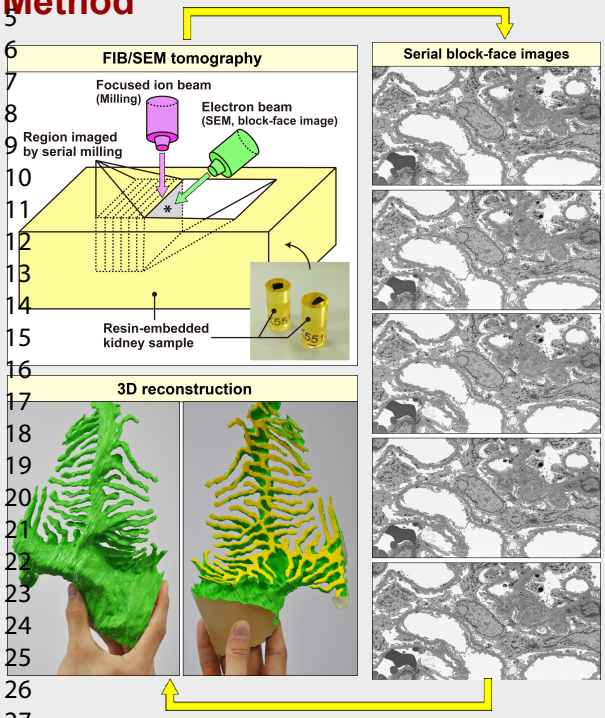

FIB/SEM images, similar to conventional TEM images, are serially acquired directly from resin-embedded samples .

Reconstructed images and models of podocytes are then produced from the serial FIB/SEM images.

Results

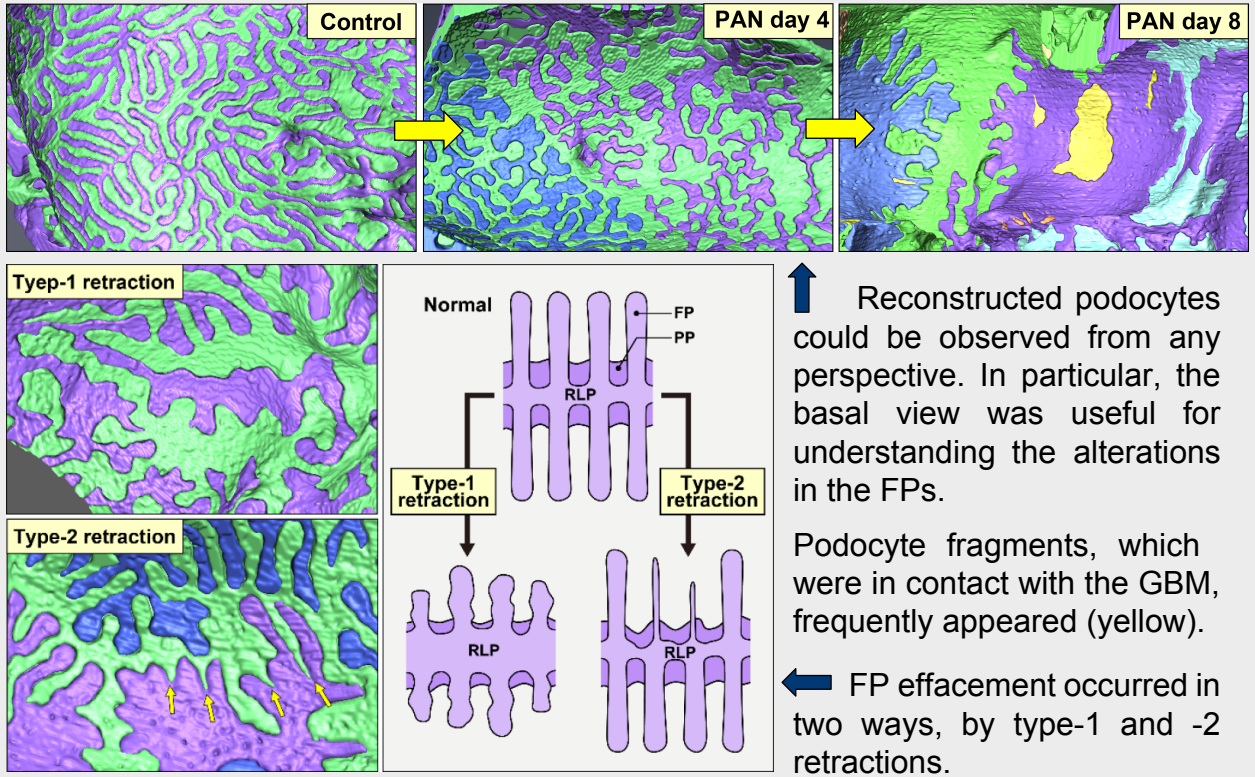

Reconstructed podocytes could be observed from any perspective. In particular, the basal view was useful for understanding the alterations in the FPs.

Podocyte fragments, which were in contact with the GBM, frequently appeared (yellow).

FP effacement occurred in two ways, by type-1 and -2 retractions.

Conclusion

FIB/SEM tomography was a powerful tool for understanding the 3D architecture of podocytes. Using this method, we more clearly and precisely clarified the morphological processes involved in FP effacement.

doi: 10.1681/ASN.

JASN
JOURNAL OF THE AMERICAN SOCIETY OF NEPHROLOGY